

CoRe3D: Collaborative Reasoning as a Foundation for 3D Intelligence

Tianjiao Yu, Xinzhuo Li, Yifan Shen, Yuanzhe Liu, Ismini Lourentzou

{ty41, lourent2}@illinois.edu

University of Illinois Urbana-Champaign

Abstract. Recent advances in large multimodal models suggest that explicit reasoning mechanisms play a critical role in improving model reliability, interpretability, and cross-modal alignment. While such reasoning-centric approaches have been proven effective in language and vision tasks, their extension to 3D remains underdeveloped. CoRe3D introduces a unified 3D understanding and generation reasoning framework that jointly operates over semantic and spatial abstractions, enabling high-level intent inferred from language to directly guide low-level 3D content formation. Central to this design is a spatially grounded reasoning representation that decomposes 3D latent space into localized regions, allowing the model to reason over geometry in a compositional and procedural manner. By tightly coupling semantic chain-of-thought inference with structured spatial reasoning, CoRe3D produces 3D outputs that exhibit strong local consistency and faithful alignment with linguistic descriptions.

1. Introduction

Despite rapid progress in 3D generation, most existing methods remain imitation-based, reproducing shapes rather than reasoning about objects [52, 105]. As a result, they struggle with prompts that implicitly describe relations, counts, geometry, or physical contacts, concepts that recent unified language-vision models have begun to handle effectively in 2D settings [69, 98]. This progress is largely attributed to the integration of Chain-of-Thought (CoT) reasoning [81], which, when extended to multimodal LLMs [7, 50, 109, 112], improves interpretability and consistency across visual reasoning tasks [34, 48].

However, unified reasoning in the 3D domain remains under-explored; few models are capable of jointly interpreting and constructing 3D objects [80, 104]. To advance this frontier, we propose **CoRe3D**, a framework for collaborative reasoning that unifies semantic understanding and geometric generation within a single 3D-LLM. As illustrated in Fig. 1, CoRe3D integrates a unified 3D language model with an octant-based 3D VQ-VAE, enabling the model to reason in both language and 3D token space.

At its core, our approach couples a **Semantic CoT** for high-level textual planning with a novel **Geometric CoT** for spatial synthesis. The geometric

CoT operates autoregressively across octant blocks, addressing the limitations of existing “flat” voxel representations that waste computation on empty space and fail to capture structured spatial dependencies. Unlike part-level representations [9], which require fixed ontologies and suffer from poor generalization across categories, or voxel-level representations [53, 90], which remain unstructured and semantically agnostic, our octant-based representation remains ontology-free yet structure-aware.

To jointly refine both reasoning streams, we further employ Group-Relative Policy Optimization (GRPO) [60], allowing CoRe3D to learn from multi-critic feedback that balances semantic intent, visual quality, and physical coherence. This reasoning-aware framework produces high-fidelity 3D construction with enhanced spatial understanding while maintaining strong general language abilities. This approach is essential for three reasons: (1) it elicits plans where no “gold” supervision exists; (2) it allows for granular process credit assignment using dense 3D-specific rewards; and (3) it prevents reward hacking and overfitting by leveraging an ensemble of different critics. By rewarding both linguistic reasoning and 3D synthesis, our approach lays the groundwork for general 3D intelligence, unifying understanding and generation.

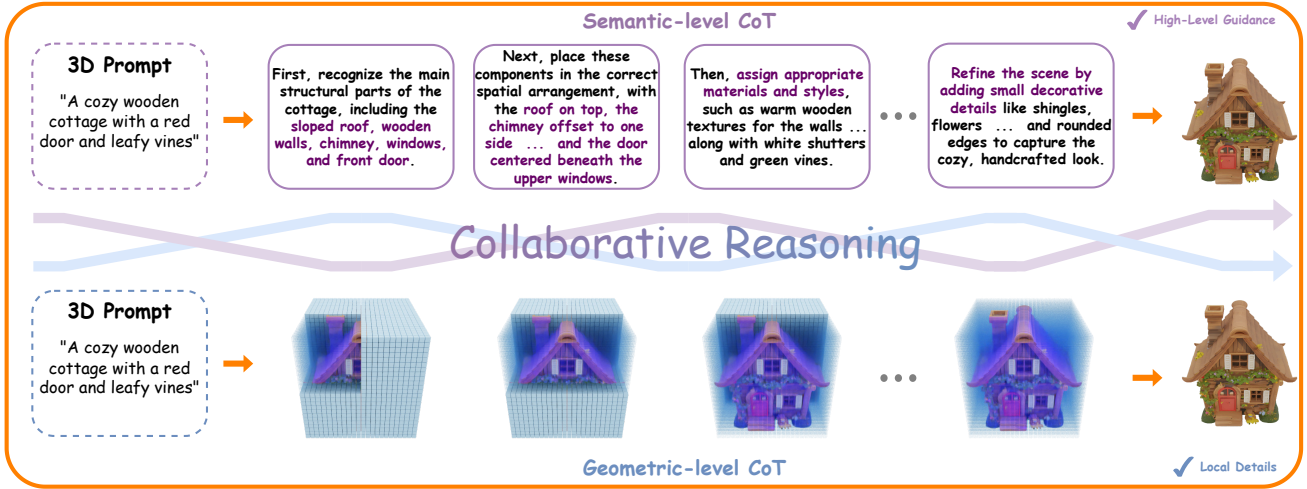


Figure 1: We introduce **CoRe3D**, a framework that unifies **Semantic CoT** and octant-based **Geometric CoT** through collaborative reasoning. By coupling language-grounded reasoning with shape constructions, CoRe3D enables bidirectional capability in both 3D understanding and generation, allowing the model to interpret objects and construct them within a unified framework.

Contributions: In summary, our contributions are:

- We introduce **CoRe3D**, a collaborative reasoning framework that unifies two complementary reasoning levels, a **Semantic CoT** for textual planning, with a novel octant-based **Geometric CoT** that acts as a structure-aware yet ontology-free prior, enabling interpretable progressive construction without category-specific part definitions.
- To the best of our knowledge, we are the first to use Co-GRPO to jointly optimize semantic and geometric reasoning in 3D. This approach elicits plans without direct supervision and effectively assigns credit using dense 3D-specific rewards (e.g., symmetry, physical coherence) for improved alignment, structure, and robustness.
- We further demonstrate that our unified reasoning paradigm is not limited to generation but naturally extends to reciprocal 3D understanding tasks, such as 3D-to-text captioning, highlighting its potential as a scalable foundation for general 3D intelligence.

2. Related Work

3D Generation. Early text-to-3D frameworks [10, 18, 35, 37, 52, 55, 64, 66, 72, 79, 105] formulated 3D synthesis as an optimization problem guided by 2D priors through score distillation sampling

(SDS). While this approach enabled cross-modal 3D generation without paired data, it required long per-instance optimization and often produced view-inconsistent geometry. Subsequent methods [8, 54, 62, 73, 78, 103] address view inconsistency by enforcing cross-view semantic constraints within diffusion pipelines. Other works address the inefficiency of iterative optimization [19, 24, 39, 43, 44, 45, 47, 61, 71, 83, 86, 101, 108, 113] by first generating consistent 2D renderings then reconstructing the 3D geometry through fast neural reconstruction.

More recently, native 3D diffusion models [16, 32, 36, 76, 87, 90, 99, 102, 110, 115] shifted toward generative modeling within latent 3D spaces, employing VAE-based encoders to learn volumetric or implicit shape priors. In contrast to diffusion models, approaches employ vector-quantized autoencoders [70], casting 3D generation as an autoregressive sequence modeling problem [13, 63, 84]. Later works [12, 14, 27, 67, 80, 85, 114] introduce task-specific tokenization schemes that directly encode vertex-face structures, improving geometric fidelity and local continuity. However, these models still operate as next-token predictors and do not expose an explicit reasoning process. Our method instead pairs an octant-based 3D VQ-VAE with a unified 3D-LLM that performs both semantic and geometric chain-of-

thought reasoning, leading to better 3D generation and understanding performance.

Unified Generation & Understanding. Recent multimodal LLMs have revealed remarkable capability in jointly processing and generating vision–language content. Early frameworks [1, 2, 17] extend LLMs with visual encoders for grounded perception, while more recent systems [40, 68, 77, 91, 116] integrate text and image generation through learned visual tokenizers and mixed-modality training.

Extending this paradigm to 3D, emerging studies [11, 29, 53, 94, 95] adapt LLMs for 3D understanding using point-cloud or shape embeddings. While effective for perception tasks, these models largely focus on recognition rather than generation. Subsequent efforts [15, 80, 104, 106, 117] attempt to unify language and 3D modeling by developing generative LLMs that handle both understanding and generation within a shared representation space. More interactive paradigms, such as LL3M [49] and L3GO [97], employ agent-based reasoning to iteratively construct or edit 3D scenes, yet rely on symbolic planning rather than token-level 3D reasoning. In contrast, our approach integrates semantic and geometric reasoning within a unified 3D-LLM. By explicitly modeling the reasoning process across both language and 3D token spaces, CoRe3D achieves reasoning-aware 3D understanding and generation, bridging the gap between linguistic intent and physically grounded 3D synthesis.

3. Method

3.1. Preliminaries

Reinforcement learning has recently become a dominant tool for eliciting reasoning behaviors in large models. A particularly effective variant is Group Relative Policy Optimization (GRPO) [60], which modifies Policy Proximal Optimization (PPO) by discarding the explicit value function and instead normalizing rewards within a sampled group of trajectories.

Formally, given a prompt–answer pair (p, a) , the old policy $\pi_{\theta_{\text{old}}}$ generates a group of G candidate responses $\{o_i\}_{i=1}^G$. Each response is scored by a

reward model, yielding \mathcal{R}_i . To reduce variance and emphasize relative quality, the advantage of the i -th response is defined by standardizing rewards within the group:

$$A_i = \frac{\mathcal{R}_i - \mu(\{\mathcal{R}_j\}_{j=1}^G)}{\sigma(\{\mathcal{R}_j\}_{j=1}^G)}, \quad (1)$$

where μ and σ denote the mean and standard deviation. The learning objective follows the clipped surrogate structure of PPO, but with a direct KL penalty that anchors the updated policy π_{θ} to a reference distribution $\pi_{\theta_{\text{ref}}}$:

$$\mathcal{J}_{\text{GRPO}}(\theta) = \mathbb{E}_{(\{o_i\}_{i=1}^G)} \left[\frac{1}{\sum_{i=1}^G |o_i|} \sum_{i=1}^G \sum_{t=1}^{|o_i|} \left(\min(r_{i,t}(\theta) A_i, \text{clip}(r_{i,t}(\theta), 1 - \varepsilon, 1 + \varepsilon) A_i) - \beta D_{\text{KL}}(\pi_{\theta} \parallel \pi_{\theta_{\text{ref}}}) \right) \right], \quad (2)$$

where the importance ratio at each token step is

$$r_{i,t}(\theta) = \frac{\pi_{\theta}(o_{i,t} \mid p, o_{i,<t})}{\pi_{\theta_{\text{old}}}(o_{i,t} \mid p, o_{i,<t})}. \quad (3)$$

Here, ε controls the clipping range of the importance ratio, and β determines the strength of the KL penalty that keeps the updated policy close to the reference policy $\pi_{\theta_{\text{ref}}}$.

While GRPO has been applied mainly in text reasoning (e.g., math or code generation), its principle of *relative quality comparison* remains under-explored in 3D generation. Leveraging this idea, we evaluate groups of rollout trajectories—spanning both semantic plans and geometric refinements—against one another, where their relative ranking provides a stable optimization signal that aligns outputs with semantic intent and geometric plausibility.

Octree-based Autoregressive Model. Recent 3D transformers such as OctFormer [74] demonstrate that representing 3D data using an *octree hierarchy* enables efficient global reasoning while preserving local geometric detail. Instead of processing dense voxel grids, an octree partitions the 3D space into hierarchical cubic cells (octants) of adaptive resolution, allocating finer subdivisions in geometrically complex regions and coarser ones in uniform areas.

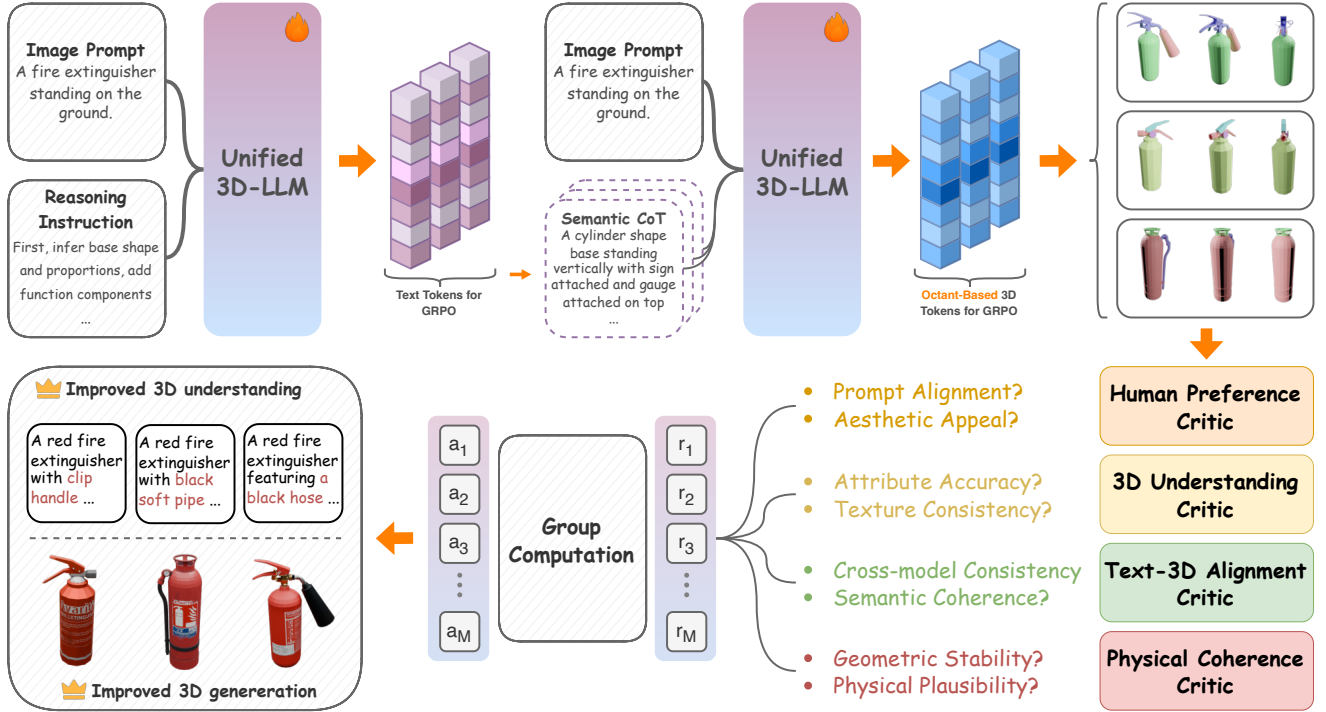


Figure 2: CoRe3D overview. Semantic and geometric reasoning tokens are generated by our unified 3D-LLM, and the generated 3D object and corresponding multiviews are evaluated by an ensemble of critics.

This sparse yet structured representation significantly reduces memory and computation costs compared to dense attention over all voxels.

Formally, an octree representation can be described as a set of hierarchical nodes $\mathcal{O} = \{o_\ell^k \mid \ell \in [0, L), k \in \mathcal{I}_\ell\}$, where ℓ denotes the level in the tree and k indexes the spatial position at that level. Each node o_ℓ^k encodes geometric and visual features (e.g., occupancy, color, or normal) aggregated from its eight child nodes at level $\ell+1$. The model applies transformer attention hierarchically across this structure: *intra-level attention* aggregates context among nodes within the same resolution, while *inter-level attention* propagates information between parent and child nodes to capture cross-scale dependencies.

This design provides two key advantages: (1) it maintains spatial locality, allowing the model to focus computation on occupied regions, and (2) it establishes a natural coarse-to-fine reasoning pathway across the 3D volume. In our work, we adopt a simplified variant of this idea by discretizing the latent 3D volume into uniform $2 \times 2 \times 2$ octant blocks rather than

an adaptive octree hierarchy. Each octant token thus serves as a fixed-resolution counterpart to an octree node, preserving the locality of the model while enabling autoregressive reasoning through the geometric CoT process described in the following sections.

3.2. Semantic and Geometric Representations

Semantic-Level Representation. A core challenge in 3D generation is translating open-ended language into structured reasoning signals that preserve compositional semantics and physical constraints. Directly mapping prompts into latent 3D tokens is under-specified, as language descriptions typically omit precise geometric, relational, and material cues, resulting in generated shapes that capture coarse appearance but fail to recover consistent structure or texture details. To address this gap, we introduce a *semantic CoT* reasoning stage that expands each textual prompt into an explicit structural plan before geometry generation. Given an input description and an optional reasoning instruction, the unified 3D-LLM first produces a detailed natural language description of the object category, spatial layout,

materials, and appearance details. This description serves as an interpretable, text-based scaffold that anchors the subsequent geometric reasoning process. Formally, we represent the semantic reasoning trace as a sequence of tokens $\mathcal{S}_{\text{sem}} = [s_1, s_2, \dots, s_N]$, conditioned on the image prompt and reasoning instruction. These tokens are optimized jointly with 3D generation tokens, enabling semantic intent to directly modulate spatial synthesis during training.

Geometric-Level Representation. We represent each 3D object using a 64^3 voxel grid, which provides a balanced trade-off between spatial fidelity and computational efficiency. To obtain a compact token representation, a 3D VQ-VAE encoder maps the voxel grid to a 16^3 latent grid, preserving local geometry and appearance features. The latent grid is serialized into 4096 latent vectors, each corresponding to a spatial location. To further reduce sequence length, we group every $2 \times 2 \times 2$ neighborhood of latent voxels (eight adjacent cells) by concatenating their channels into a single vector. This operation transforms the 4096 latent vectors (with 8-D channels) into 512 tokens with 64-D channels, where each token represents a local *octant block* within the 3D volume.

A vector-quantization module with an 8192-entry codebook discretizes these octant features, resulting in 512 discrete 3D tokens per object. For spatial disambiguation across blocks, we attach a learned absolute position embedding to each octant token, keyed by its (x_b, y_b, z_b) index on the $8 \times 8 \times 8$ block grid (or an equivalent Morton/Z-order code). This embedding is injected post-quantization, so the codebook remains content-centric while the generator remains location-aware.

This octant-based representation naturally supports our *geometric CoT* reasoning: the model iteratively “thinks” over octant tokens, refining or sampling candidate completions for each sub-cube. We denote the sequence of geometric reasoning tokens as

$$\mathcal{G}_{\text{geo}} = [g_1, g_2, \dots, g_M], \quad (4)$$

where each token g_i corresponds to a discrete octant block produced by the 3D VQ-VAE. While the *semantic CoT* \mathcal{S}_{sem} expresses the conceptual plan in language space, the *geometric CoT* \mathcal{G}_{geo} realizes that

plan token-by-token in the 3D latent space. Together, these two reasoning levels enable controllable and interpretable 3D generation that preserves both global semantics and local geometric precision.

3.3. Collaborative Reasoning

The core innovation of our framework lies in the explicit collaboration between *semantic* and *geometric* reasoning. While each level can operate independently, its joint optimization leads to stronger, mutually reinforcing behavior. We unify them through **3D Co-GRPO**, a reinforcement learning framework that refines both reasoning levels using multi-critic 3D-aware rewards, aligning linguistic intent with spatial construction. This results in objects that are semantically faithful, visually compelling, and physically coherent. An overview is shown in fig. 2.

Formally, given an input prompt T_p and pre-generated semantic CoT decoded from \mathcal{S}_{sem} , the unified 3D-LLM produces a geometric reasoning sequence $\mathcal{G}_{\text{geo}} = [g_1, g_2, \dots, g_M]$ to synthesize the final 3D object \hat{O} . The process can be viewed as a sequential reasoning pipeline: the semantic trace \mathcal{S}_{sem} provides global planning cues such as object category, spatial relations, and texture details, while the geometric trace \mathcal{G}_{geo} progressively realizes those cues within the latent 3D token space.

We extend the Generalized Reinforcement Preference Optimization (GRPO) paradigm into the 3D domain by introducing four complementary *critics*, each providing a scalar reward that captures a distinct dimension of 3D quality. The resulting meshes and multi-view renderings $\{I_i\}$ are evaluated by an ensemble of 3D experts:

- **Human Preference Critic:** evaluates perceptual realism and human aesthetic preference, assessing prompt relevance and overall visual appeal from multi-view renderings [88, 93, 103].
- **3D Understanding Critic:** verifies attribute- and part-level correctness using 3D-VQA models [11, 29, 53, 117] that query geometric, textural, and symmetry attributes derived from the semantic CoT \mathcal{S}_{sem} .
- **Text-3D Alignment Critic:** measures semantic faithfulness between the textual reasoning trace (prompt and \mathcal{S}_{sem}) and the generated geometry

\mathcal{G}_{geo} , using pretrained text–3D embedding models [96, 106] to ensure cross-modal coherence and faithful alignment.

- **Physical Coherence Critic:** analytically enforces structural stability and physical plausibility through a differentiable reward composed of three geometry-based terms: $R_P = \lambda_1 R_{\text{stab}} + \lambda_2 R_{\text{rig}} + \lambda_3 R_{\text{int}}$, where R_{stab} measures global balance of the center of mass, R_{rig} promotes topologically connected geometry that maintains physical continuity, and R_{int} penalizes self-intersection between surfaces. This critic is fully geometry-driven and provides a compact measure of physical coherence.

Each critic outputs a normalized reward $R_i \in [0, 1]$, and the overall GRPO objective aggregates them via

$$R = w_H R_H + w_V R_V + w_X R_X + w_P R_P, \quad (5)$$

where weights balance human preference, 3D understanding, cross-modal alignment, and physical coherence. The combined reward provides preference signals for policy updates, encouraging the model to improve both reasoning accuracy and geometric fidelity over GRPO iterations.

During training, the model first performs forward generation to produce \mathcal{S}_{sem} and \mathcal{G}_{geo} for each prompt T_p . Generated results are rendered into multi-view images and passed through the four critics, producing individual rewards $\{R_H, R_V, R_X, R_P\}$. The composite reward in Eq. (5) is then used to compute pairwise preferences among samples and update the model using the GRPO objective defined in Eq. (2).

4. Experiments

Implementation Details. Our training data is sourced from the 3D-Alpaca dataset [104], which comprises approximately 2.56M multimodal samples spanning text-to-3D, image-to-3D, 3D-captioning, and 3D-editing tasks. Each 3D asset is rendered from four orthogonal views and paired with GPT-generated captions, providing rich interleaved supervision across modalities. We initialize our 3D-ULM from ShapeLLM-Omni [104], which we extend with our octant-based 3D VQ-VAE for compact geometry representation and geometric CoT reasoning.

Table 1: Evaluation of general conversational and reasoning abilities on standard language benchmarks. We compare CoRe3D against top-tier general vision-language models (VLMs) and 3D-specific language models. Our model demonstrates SoTA or competitive language understanding and reasoning performance. **Best** and **second-best** are highlighted.

Benchmark	Qwen2.5-vl-7B	LLaMA3.2-Vision-11B	LLaMA-Mesh-8B	ShapeLLM-Omni-7B	CoRe3D
MMLU \uparrow	67.5	66.2	59.8	64.3	67.6
PIQA \uparrow	81.3	80.1	79.8	78.9	79.4
GSM8K \uparrow	43.2	42.1	37.2	55.6	57.3
SIQA \uparrow	41.0	40.6	40.3	41.5	41.5

Training follows the 3D Co-GRPO framework with a base learning rate of 1×10^{-6} and KL regularization $\beta = 0.01$. The model is trained for 40k steps with batch size 256 on 8×L40 GPUs.

For reward computation, we render multi-view images for each generated mesh and evaluate them using HPS [88] for the Human Preference Critic, ShapeLLM [53] for the 3D Understanding Critic, and ULIP [96] embeddings for the Text–3D Alignment Critic. Finally, the Physical Coherence Critic is implemented through geometry-based evaluation on the generated meshes. Given each generated mesh. All critic scores are normalized to $[0, 1]$ and fused as in Eq. 5 to guide policy optimization under the GRPO objective (Eq. 2). More details in the Appendix.

4.1. Quantitative Results

General Conversational Abilities. We first evaluate the foundational language understanding of CoRe3D. We compare against leading general-purpose VLMs (Qwen2.5-vl-7B [98], LLaMA3.2-Vision-11B [69]) and 3D-focused multimodal models (LLaMA-Mesh-8B [80], ShapeLLM-Omni-7B [104]) on a suite of standard language benchmarks. These include MMLU [28], PIQA [6], GSM8K [20], and SIQA [58]. As shown in Table 1, CoRe3D maintains its general conversational abilities with good language understanding and reasoning performance. These results suggest that our co-reasoning mechanism does not diminish the model’s broader reasoning capabilities but instead strengthens them.

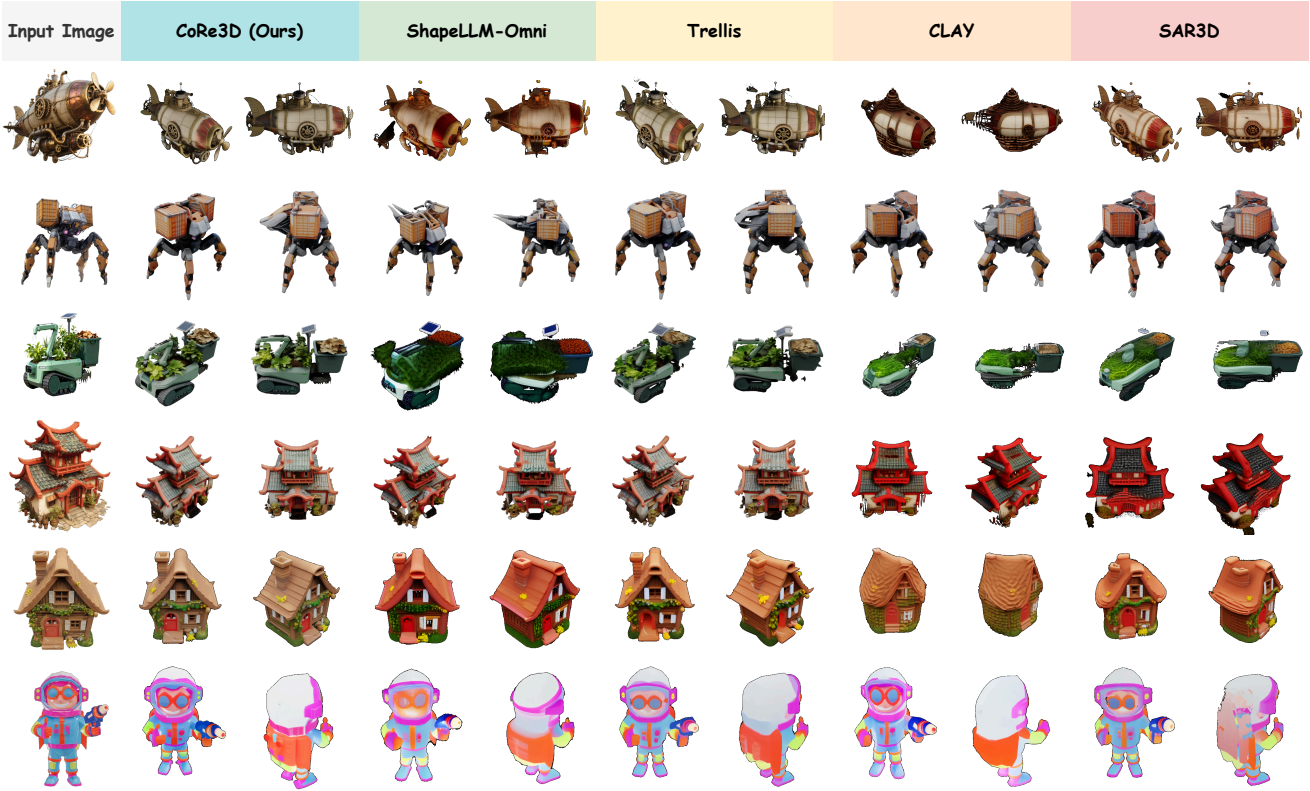


Figure 3: Image-to-3D qualitative comparison. Given a single input image, CoRe3D produces 3D shapes with higher geometric fidelity, cleaner topology, and stronger semantic alignment compared to baselines.

Table 2: 3D object captioning results on the Objaverse benchmark. We evaluate the model’s 3D caption capability. CoRe3D achieves state-of-the-art performance by a significant margin across all n-gram and semantic similarity metrics, demonstrating that our reasoning-driven generative training directly enhances 3D understanding. **Best** and **second-best** results are highlighted.

Model	BLEU-1 ↑	ROUGE-L ↑	METEOR ↑	Sentence-BERT ↑	SimCSE ↑
LLaVA-13B	4.01	8.18	13.18	46.97	48.86
Qwen2.5-vl-7B	4.05	7.85	14.23	48.90	50.86
3D-LLM	15.11	17.84	19.22	42.36	43.58
LEO	16.98	20.12	20.91	48.01	47.25
PointLLM-13B	3.18	7.54	12.24	47.89	49.01
ShapeLLM-Omni	18.92	21.46	22.12	49.43	50.72
CoRe3D	24.02	26.45	24.98	51.17	52.79

3D object Understanding. Beyond general language abilities, a key goal of our work is to excel at 3D understanding. We test this reciprocal capability using the 3D object captioning task on the Objaverse [21] dataset. We compare CoRe3D against prominent general-purpose VLMs (LLaVA-13B [41], Qwen2.5-vl-7B) and specialized 3D-language models (3D-

Table 3: Quantitative comparison of 3D generation quality for Text-to-3D and Image-to-3D tasks. We evaluate CoRe3D against state-of-the-art generative models. Results show CoRe3D achieves competitive performance on all metrics for both tasks. **Best** and **second-best** results are highlighted.

Method	Text-to-3D			Image-to-3D		
	CLIP ↑	FD _{incep} ↓	KD _{incep} ↓	CLIP ↑	FD _{incep} ↓	KD _{incep} ↓
SAR3D	23.1	28.4	0.27	83.9	22.1	0.18
CLAY	27.3	23.9	0.21	84.6	13.5	0.10
Trellis	28.9	18.6	0.19	85.1	10.9	0.08
ShapeLLM-Omni	27.0	24.4	0.24	84.4	14.1	0.09
CoRe3D	30.4	18.5	0.18	85.9	11.2	0.08

LLM [29], LEO [30], PointLLM-13B [94], ShapeLLM-Omni [104]). Performance is measured using n-gram matching (BLEU-1, ROUGE-L, METEOR) and semantic embedding similarity (Sentence-BERT, SimCSE) following the evaluation settings in PointLLM. The results in Table 2 show that CoRe3D decisively outperforms all baselines across all five metrics. These results quantitatively confirm that our co-reasoning method substantially improves 3D understanding.

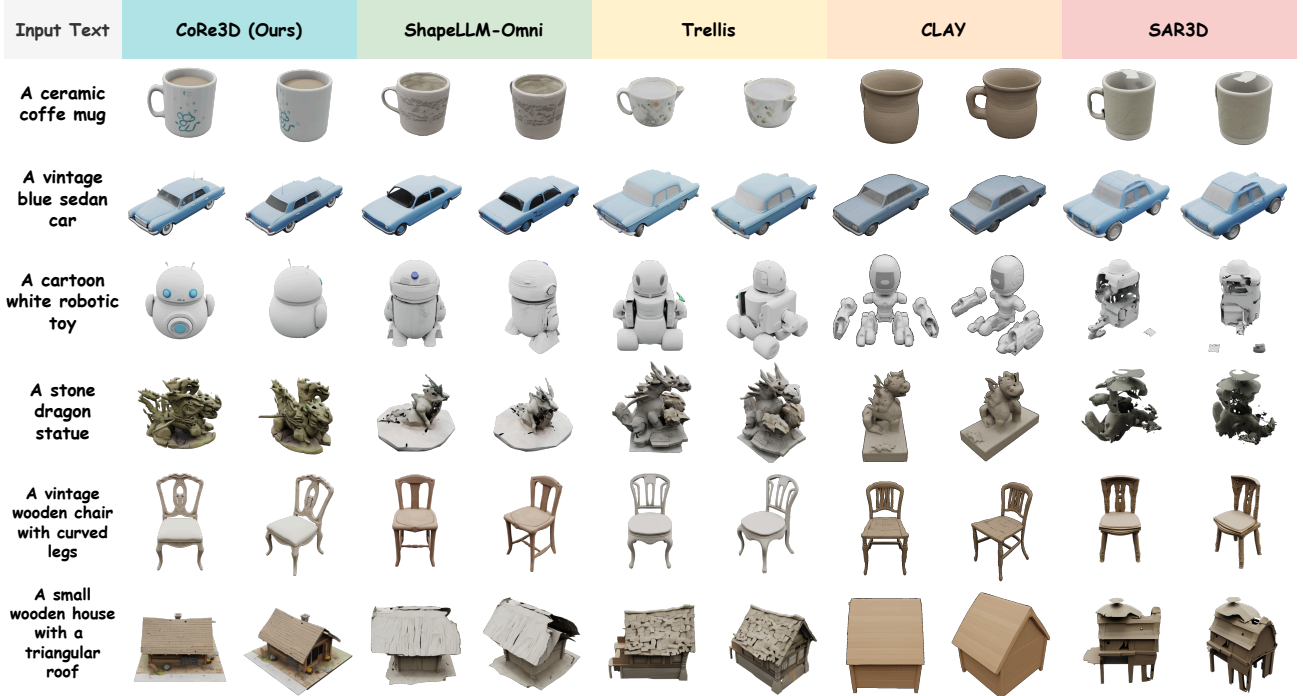


Figure 4: Text-to-3D qualitative comparison. CoRe3D generates 3D objects that more faithfully follow the textual prompt.

3D-Generation. We evaluate the core generative capabilities of CoRe3D on both Text-to-3D and Image-to-3D synthesis. We compare against several leading methods, including SAR3D [15], CLAY [110], Trellis [90], and ShapeLLM-Omni [104]. We use three standard metrics: CLIP Score, Frechet Distance (FD), and Kernel Distance (KD) to assess the generation quality. As shown in Table 3, our method achieves state-of-the-art results in the Text-to-3D task, demonstrating a clear gain by ranking first across all three metrics. Our high CLIP score is a direct quantitative validation of our core contribution: the Semantic CoT, jointly optimized with GRPO and a Text-3D Alignment Critic, successfully made our model more faithful to the text. This strong performance extends to Image-to-3D generation, where our model leads in prompt alignment (CLIP 85.9) and maintains promising quality compared to the state-of-the-art 3D generation-only models.

4.2. Qualitative results

Standard 3D Generation. We first evaluate CoRe3D on standard image-to-3D and text-to-3D tasks, com-

paring it against strong baselines, including the unified 3D models ShapeLLM-Omni [104] and SAR3D [15], as well as the generation-focused models Trellis [90] and CLAY [110]. As illustrated in Figure 3, competing methods often exhibit misalignment with the input image or suffer from geometric artifacts. In contrast, our model generates 3D meshes with high geometric fidelity and semantic coherence, faithfully capturing the complex structures present in the source image. This superior performance extends to text-to-3D generation, as shown in Figure 4. Our model achieves a more robust alignment with the text prompt. Notably, CoRe3D successfully interprets and renders fine-grained stylistic details, such as the “cartoon” attribute, producing 3D meshes that align precisely with the prompt’s intention.

Reasoning-based 3D Generation. The robust understanding capabilities of CoRe3D unlock a more challenging class of 3D generation: synthesis from complex or indirect prompts. These prompts often require world knowledge and compositional reasoning to infer the user’s true intent (e.g., inferring “Statue of Liberty” from “A colossal copper figure holding a torch ... symbolizing freedom and hope”).

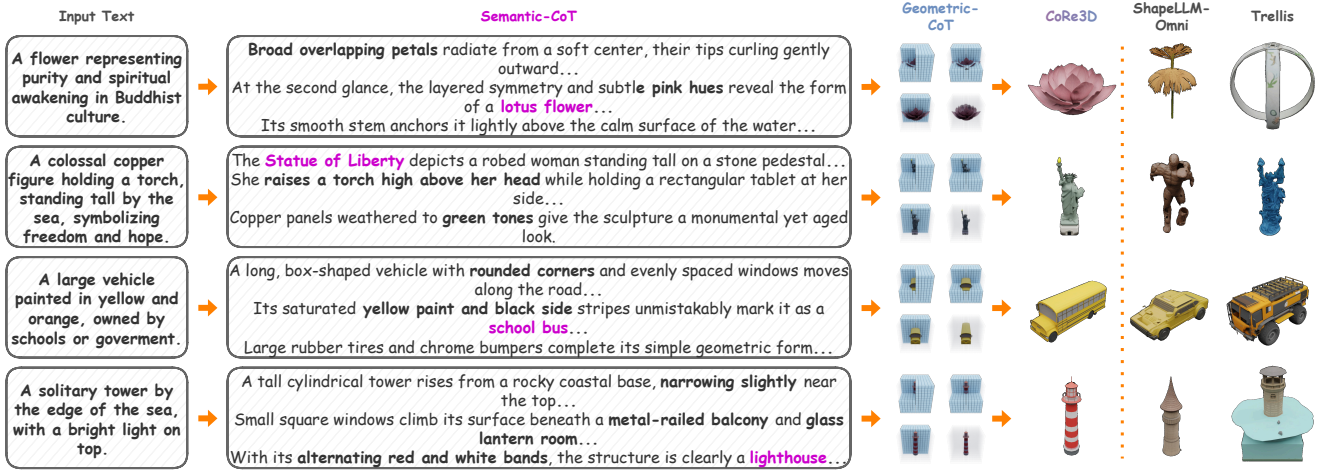


Figure 5: Qualitative results of CoRe3D on challenging prompts that require inferring the correct object or interpreting implicit descriptive cues. Comparing with the base model ShapeLLM-Omni [104] and state-of-the-art generation model Trellis [90], our model successfully inferred the true object from the implicit prompts. (e.g., “a colossal copper figure holding a torch ... symbolizing freedom and hope” corresponds to *The Statue of Liberty*.)



Figure 6: Qualitative results on 3D part editing. The collaborative reasoning in our framework enhances instruction comprehension, yielding edits that align more faithfully with the input text and produce 3D shapes that accurately reflect the specified modifications.

Standard models, which lack an explicit reasoning stage, fail at this task, generating literal but semantically incorrect shapes. As demonstrated in Figure 5, CoRe3D successfully navigates these challenges. Our model’s Semantic-CoT first deconstructs the ambiguous prompt into a structured steps and effectively infers the underlying intention, allowing our model to produce 3D objects that maintain high faithfulness to the prompt’s true meaning.

3D Part Editing. Compared with traditional generative models, unified 3D LMs unlock a powerful language-driven paradigm for interactive 3D asset



Figure 7: Ablating Semantic CoT and Geometric CoT compared against CoRe3D and ShapeLLM-Omni [104]. Results show both CoT contribute significantly towards the final performance.

manipulation. As shown in Figure 6, our model can perform fine-grained part-level edits while preserving object identity and structural coherence. Additional results are provided in the Appendix.

4.3. Ablations

Semantic-CoT and Geometric-CoT. We ablate CoRe3D by removing either the Semantic-CoT tokens or the Geometric-CoT tokens for the GRPO pipeline. As shown in Figure 7, removing Semantic-CoT leads to structurally plausible objects but lacks category- and attribute-specific cues. Conversely, removing

Table 4: Ablation of different critics. HP, 3DU, TA, and PC correspond to Human Preference, 3D Understanding, Text-3D Alignment, and Physical Coherence respectively. **Best** and **second-best** results are highlighted.

Critic				3D Captioning			3D Generation		
HP	3DU	TA	PC	METEOR \uparrow	Sentence-BERT \uparrow	SimCSE \uparrow	CLIP \uparrow	FD _{insep} \downarrow	KD _{insep} \downarrow
✓	-	-	-	12.76	44.91	48.14	0.29	23.4	0.25
-	✓	-	-	14.12	47.88	49.63	0.31	22.7	0.23
-	-	✓	-	15.34	46.52	50.11	0.33	21.9	0.21
-	-	-	✓	13.41	45.76	48.62	0.30	20.8	0.22
-	✓	✓	-	18.92	48.77	51.24	0.36	19.7	0.19
✓	-	✓	✓	20.48	49.02	51.89	0.37	19.9	0.20
✓	✓	-	-	19.83	49.88	51.01	0.38	20.1	0.19
✓	✓	✓	-	21.55	50.41	51.43	0.37	19.4	0.20
✓	✓	✓	✓	24.98	51.17	52.79	0.40	18.5	0.18

Geometric-CoT results in objects with clear geometric distortions and simplified shapes.

Reward analysis We analyze the role of each critic and their combinations to better understand how different reward signals shape model behavior. As shown in Table 4, each critic contributes complementary improvements. Text-3D alignment yields the largest gains in caption quality, showing its importance for accurate descriptions. 3D Understanding significantly improves generation quality by enforcing stronger object-level structure. Combining multiple critics steadily improves performance: pairs such as (3DU + TA + PC) or (HP + TA + PC) achieve balanced improvements across both captioning and generation tasks. More details in the Appendix

5. Conclusion

We introduce CoRe3D, a collaborative reasoning framework that unifies semantic planning and geometric construction through a dual chain-of-thought process. By coupling these complementary reasoning levels and optimizing them jointly with 3D Co-GRPO, our model achieves state-of-the-art performance across both 3D generation and understanding tasks. Beyond producing faithful and physically coherent 3D assets, CoRe3D demonstrates robust interpretive capabilities, successfully handling indirect and referring descriptions, ambiguous prompts, and fine-grained part-level edits. Our results highlight collaborative reasoning as a scalable and structure-aware foundation for general 3D intelligence.

References

- [1] Jean-Baptiste Alayrac, Jeff Donahue, Pauline Luc, Antoine Miech, Iain Barr, Yana Hasson, Karel Lenc, Arthur Mensch, Katherine Millican, Malcolm Reynolds, et al. Flamingo: a visual language model for few-shot learning. *Advances in neural information processing systems*, 35:23716–23736, 2022.
- [2] Jinze Bai, Shuai Bai, Yunfei Chu, Zeyu Cui, Kai Dang, Xiaodong Deng, Yang Fan, Wenbin Ge, Yu Han, Fei Huang, et al. Qwen technical report. *arXiv preprint arXiv:2309.16609*, 2023.
- [3] Shuai Bai, Keqin Chen, Xuejing Liu, Jialin Wang, Wenbin Ge, Sibong Song, Kai Dang, Peng Wang, Shijie Wang, Jun Tang, et al. Qwen2. 5-vl technical report. *arXiv preprint arXiv:2502.13923*, 2025.
- [4] Satantjeev Banerjee and Alon Lavie. Meteor: An automatic metric for mt evaluation with improved correlation with human judgments. In *Proceedings of the acl workshop on intrinsic and extrinsic evaluation measures for machine translation and/or summarization*, pages 65–72, 2005.
- [5] David Benson and Joel Davis. Octree textures. *ACM Transactions on Graphics (TOG)*, 21(3): 785–790, 2002.
- [6] Yonatan Bisk, Rowan Zellers, Jianfeng Gao, Yejin Choi, et al. Piqa: Reasoning about physical commonsense in natural language. In *Proceedings of the AAAI conference on artificial intelligence*, volume 34, pages 7432–7439, 2020.
- [7] Liang Chen, Lei Li, Haozhe Zhao, Yifan Song, and Vinci. R1-v: Reinforcing super generalization ability in vision-language models with less than \$3. <https://github.com/Deep-Agent/R1-V>, 2025. Accessed: 2025-02-02.
- [8] Luxi Chen, Zhengyi Wang, Chongxuan Li, Tingting Gao, Hang Su, and Jun Zhu. Mi-

- crodreamer: Zero-shot 3d generation in 20 seconds by score-based iterative reconstruction. *arXiv e-prints*, pages arXiv-2404, 2024.
- [9] Minghao Chen, Jianyuan Wang, Roman Shapovalov, Tom Monnier, Hyunyoung Jung, Dilin Wang, Rakesh Ranjan, Iro Laina, and Andrea Vedaldi. Autopartgen: Autogressive 3d part generation and discovery. *arXiv preprint arXiv:2507.13346*, 2025.
- [10] Rui Chen, Yongwei Chen, Ningxin Jiao, and Kui Jia. Fantasia3d: Disentangling geometry and appearance for high-quality text-to-3d content creation. In *Proceedings of the IEEE/CVF international conference on computer vision*, pages 22246–22256, 2023.
- [11] Sijin Chen, Xin Chen, Chi Zhang, Mingsheng Li, Gang Yu, Hao Fei, Hongyuan Zhu, Jiayuan Fan, and Tao Chen. Ll3da: Visual interactive instruction tuning for omni-3d understanding reasoning and planning. In *Proceedings of the IEEE/CVF conference on computer vision and pattern recognition*, pages 26428–26438, 2024.
- [12] Sijin Chen, Xin Chen, Anqi Pang, Xianfang Zeng, Wei Cheng, Yijun Fu, Fukun Yin, Bilzb Wang, Jingyi Yu, Gang Yu, et al. Meshxl: Neural coordinate field for generative 3d foundation models. *Advances in Neural Information Processing Systems*, 37:97141–97166, 2025.
- [13] Yiwen Chen, Tong He, Di Huang, Weicai Ye, Sijin Chen, Jiaxiang Tang, Xin Chen, Zhonggang Cai, Lei Yang, Gang Yu, et al. Meshanything: Artist-created mesh generation with autoregressive transformers. *arXiv preprint arXiv:2406.10163*, 2024.
- [14] Yiwen Chen, Yikai Wang, Yihao Luo, Zhengyi Wang, Zilong Chen, Jun Zhu, Chi Zhang, and Guosheng Lin. Meshanything v2: Artist-created mesh generation with adjacent mesh tokenization. *arXiv preprint arXiv:2408.02555*, 2024.
- [15] Yongwei Chen, Yushi Lan, Shangchen Zhou, Tengfei Wang, and Xingang Pan. Sar3d: Autoregressive 3d object generation and understanding via multi-scale 3d vqvae. In *CVPR*, 2025.
- [16] Zhaoxi Chen, Jiaxiang Tang, Yuhao Dong, Ziang Cao, Fangzhou Hong, Yushi Lan, Tengfei Wang, Haozhe Xie, Tong Wu, Shunsuke Saito, et al. 3dtopia-xl: Scaling high-quality 3d asset generation via primitive diffusion. *arXiv preprint arXiv:2409.12957*, 2024.
- [17] Zhe Chen, Jiannan Wu, Wenhai Wang, Weijie Su, Guo Chen, Sen Xing, Muyan Zhong, Qinglong Zhang, Xizhou Zhu, Lewei Lu, et al. Internvl: Scaling up vision foundation models and aligning for generic visual-linguistic tasks. In *Proceedings of the IEEE/CVF conference on computer vision and pattern recognition*, pages 24185–24198, 2024.
- [18] Zilong Chen, Feng Wang, Yikai Wang, and Huaping Liu. Text-to-3d using gaussian splatting. In *Proceedings of the IEEE/CVF conference on computer vision and pattern recognition*, pages 21401–21412, 2024.
- [19] Zilong Chen, Yikai Wang, Feng Wang, Zhengyi Wang, and Huaping Liu. V3d: Video diffusion models are effective 3d generators. *arXiv preprint arXiv:2403.06738*, 2024.
- [20] Karl Cobbe, Vineet Kosaraju, Mohammad Bavarian, Mark Chen, Heewoo Jun, Lukasz Kaiser, Matthias Plappert, Jerry Tworek, Jacob Hilton, Reiichiro Nakano, et al. Training verifiers to solve math word problems, 2021. *URL* <https://arxiv.org/abs/2110.14168>, 9, 2021.
- [21] Matt Deitke, Ruoshi Liu, Matthew Wallingford, Huong Ngo, Oscar Michel, Aditya Kusupati, Alan Fan, Christian Laforte, Vikram Voleti, Samir Yitzhak Gadre, et al. Objaverse-xl: A universe of 10m+ 3d objects. *Advances in Neural Information Processing Systems*, 36: 35799–35813, 2023.
- [22] Kangle Deng, Hsueh-Ti Derek Liu, Yiheng Zhu, Xiaoxia Sun, Chong Shang, Kiran S Bhat, Deva Ramanan, Jun-Yan Zhu, Maneesh Agrawala,

- and Tinghui Zhou. Efficient autoregressive shape generation via octree-based adaptive tokenization. In *Proceedings of the IEEE/CVF International Conference on Computer Vision*, pages 11685–11696, 2025.
- [23] Tianyu Gao, Xingcheng Yao, and Danqi Chen. Simcse: Simple contrastive learning of sentence embeddings. *arXiv preprint arXiv:2104.08821*, 2021.
- [24] Zhirui Gao, Renjiao Yi, Yuhang Huang, Wei Chen, Chenyang Zhu, and Kai Xu. Partgs: Learning part-aware 3d representations by fusing 2d gaussians and superquadrics. *arXiv preprint arXiv:2408.10789*, 2024.
- [25] Ethan Griffiths, Maryam Haghighat, Simon Denman, Clinton Fookes, and Milad Ramezani. Hotformerloc: Hierarchical octree transformer for versatile lidar place recognition across ground and aerial views. In *IEEE Conference on Computer Vision and Pattern Recognition (CVPR)*, pages 6648–6658, 2025.
- [26] Daya Guo, Dejian Yang, Haowei Zhang, Junxiao Song, Ruoyu Zhang, Runxin Xu, Qihao Zhu, Shirong Ma, Peiyi Wang, Xiao Bi, et al. Deepseek-r1: Incentivizing reasoning capability in llms via reinforcement learning. *arXiv preprint arXiv:2501.12948*, 2025.
- [27] Zekun Hao, David W Romero, Tsung-Yi Lin, and Ming-Yu Liu. Meshtron: High-fidelity, artist-like 3d mesh generation at scale. *arXiv preprint arXiv:2412.09548*, 2024.
- [28] Dan Hendrycks, Collin Burns, Steven Basart, Andy Zou, Mantas Mazeika, Dawn Song, and Jacob Steinhardt. Measuring massive multi-task language understanding. *arXiv preprint arXiv:2009.03300*, 2020.
- [29] Yining Hong, Haoyu Zhen, Peihao Chen, Shuhong Zheng, Yilun Du, Zhenfang Chen, and Chuang Gan. 3d-llm: Injecting the 3d world into large language models. *Advances in Neural Information Processing Systems*, 36: 20482–20494, 2023.
- [30] Jiangyong Huang, Silong Yong, Xiaojian Ma, Xiongkun Linghu, Puhao Li, Yan Wang, Qing Li, Song-Chun Zhu, Baoxiong Jia, and Siyuan Huang. An embodied generalist agent in 3d world, 2024. URL <https://arxiv.org/abs/2311.12871>.
- [31] Wenxuan Huang, Bohan Jia, Zijie Zhai, Shaosheng Cao, Zheyu Ye, Fei Zhao, Zhe Xu, Yao Hu, and Shaohui Lin. Vision-r1: Incentivizing reasoning capability in multi-modal large language models. *arXiv preprint arXiv:2503.06749*, 2025.
- [32] Zixuan Huang, Mark Boss, Aaryaman Vasishta, James M Rehg, and Varun Jampani. Spar3d: Stable point-aware reconstruction of 3d objects from single images. *arXiv preprint arXiv:2501.04689*, 2025.
- [33] Naman Jain, King Han, Alex Gu, Wen-Ding Li, Fanjia Yan, Tianjun Zhang, Sida Wang, Armando Solar-Lezama, Koushik Sen, and Ion Stoica. Livecodebench: Holistic and contamination free evaluation of large language models for code. *arXiv preprint arXiv:2403.07974*, 2024.
- [34] Dongzhi Jiang, Renrui Zhang, Ziyu Guo, Yanwei Li, Yu Qi, Xinyan Chen, Liuhui Wang, Jianhan Jin, Claire Guo, Shen Yan, et al. Mme-cot: Benchmarking chain-of-thought in large multimodal models for reasoning quality, robustness, and efficiency. *arXiv preprint arXiv:2502.09621*, 2025.
- [35] Weiyu Li, Rui Chen, Xuelin Chen, and Ping Tan. Sweetdreamer: Aligning geometric priors in 2d diffusion for consistent text-to-3d. *arxiv:2310.02596*, 2023.
- [36] Weiyu Li, Jiarui Liu, Rui Chen, Yixun Liang, Xuelin Chen, Ping Tan, and Xiaoxiao Long. Craftsman: High-fidelity mesh generation with 3d native generation and interactive geometry refiner. *arXiv preprint arXiv:2405.14979*, 2024.
- [37] Chen-Hsuan Lin, Jun Gao, Luming Tang, Towaki Takikawa, Xiaohui Zeng, Xun Huang,

- Karsten Kreis, Sanja Fidler, Ming-Yu Liu, and Tsung-Yi Lin. Magic3d: High-resolution text-to-3d content creation. In *Proceedings of the IEEE/CVF conference on computer vision and pattern recognition*, pages 300–309, 2023.
- [38] Chin-Yew Lin. Rouge: A package for automatic evaluation of summaries. In *Text summarization branches out*, pages 74–81, 2004.
- [39] Fangfu Liu, Wenqiang Sun, Hanyang Wang, Yikai Wang, Haowen Sun, Junliang Ye, Jun Zhang, and Yueqi Duan. Reconx: Reconstruct any scene from sparse views with video diffusion model, 2024. URL <https://arxiv.org/abs/2408.16767>.
- [40] Hao Liu, Wilson Yan, Matei Zaharia, and Pieter Abbeel. World model on million-length video and language with blockwise ringattention. *arXiv preprint arXiv:2402.08268*, 2024.
- [41] Haotian Liu, Chunyuan Li, Qingyang Wu, and Yong Jae Lee. Visual instruction tuning, 2023.
- [42] Jiawei Liu, Nirav Diwan, Zhe Wang, Haoyu Zhai, Xiaona Zhou, Kiet A Nguyen, Tianjiao Yu, Muntasir Wahed, Yinlin Deng, Hadjer Benkraouda, et al. Purpcode: Reasoning for safer code generation. *arXiv preprint arXiv:2507.19060*, 2025.
- [43] Minghua Liu, Chao Xu, Haian Jin, Linghao Chen, Mukund Varma T, Zexiang Xu, and Hao Su. One-2-3-45: Any single image to 3d mesh in 45 seconds without per-shape optimization. *Advances in Neural Information Processing Systems*, 36:22226–22246, 2023.
- [44] Ruoshi Liu, Rundi Wu, Basile Van Hoorick, Pavel Tokmakov, Sergey Zakharov, and Carl Vondrick. Zero-1-to-3: Zero-shot one image to 3d object. In *Proceedings of the IEEE/CVF international conference on computer vision*, pages 9298–9309, 2023.
- [45] Yuan Liu, Cheng Lin, Zijiao Zeng, Xiaoxiao Long, Lingjie Liu, Taku Komura, and Wenping Wang. Syncdreamer: Generating multiview-consistent images from a single-view image. *arXiv preprint arXiv:2309.03453*, 2023.
- [46] Yuan Liu, Haodong Duan, Yuanhan Zhang, Bo Li, Songyang Zhang, Wangbo Zhao, Yike Yuan, Jiaqi Wang, Conghui He, Ziwei Liu, et al. Mmbench: Is your multi-modal model an all-around player? In *European conference on computer vision*, pages 216–233. Springer, 2024.
- [47] Xiaoxiao Long, Yuan-Chen Guo, Cheng Lin, Yuan Liu, Zhiyang Dou, Lingjie Liu, Yuexin Ma, Song-Hai Zhang, Marc Habermann, Christian Theobalt, et al. Wonder3d: Single image to 3d using cross-domain diffusion. In *Proceedings of the IEEE/CVF conference on computer vision and pattern recognition*, pages 9970–9980, 2024.
- [48] Pan Lu, Hritik Bansal, Tony Xia, Jiacheng Liu, Chun yue Li, Hannaneh Hajishirzi, Hao Cheng, Kai-Wei Chang, Michel Galley, and Jianfeng Gao. Mathvista: Evaluating math reasoning in visual contexts with gpt-4v, bard, and other large multimodal models. *ArXiv*, abs/2310.02255, 2023.
- [49] Sining Lu, Guan Chen, Nam Anh Dinh, Itai Lang, Ari Holtzman, and Rana Hanocka. Ll3m: Large language 3d modelers, 2025. URL <https://arxiv.org/abs/2508.08228>.
- [50] Fanqing Meng, Lingxiao Du, Zongkai Liu, Zhixiang Zhou, Quanfeng Lu, Daocheng Fu, Botian Shi, Wenhai Wang, Junjun He, Kaipeng Zhang, et al. Mm-eureka: Exploring visual aha moment with rule-based large-scale reinforcement learning. *arXiv preprint arXiv:2503.07365*, 2025.
- [51] Kishore Papineni, Salim Roukos, Todd Ward, and Wei-Jing Zhu. Bleu: a method for automatic evaluation of machine translation. In *Proceedings of the 40th annual meeting of the Association for Computational Linguistics*, pages 311–318, 2002.
- [52] Ben Poole, Ajay Jain, Jonathan T Barron, and Ben Mildenhall. Dreamfusion: Text-to-3d using 2d diffusion. *arXiv preprint arXiv:2209.14988*, 2022.

- [53] Zekun Qi, Runpei Dong, Shaochen Zhang, Haoran Geng, Chunrui Han, Zheng Ge, Li Yi, and Kaisheng Ma. Shapellm: Universal 3d object understanding for embodied interaction. In *European Conference on Computer Vision*, pages 214–238. Springer, 2024.
- [54] Lingteng Qiu, Guanying Chen, Xiaodong Gu, Qi Zuo, Mutian Xu, Yushuang Wu, Weihao Yuan, Zilong Dong, Liefeng Bo, and Xiaoguang Han. Richdreamer: A generalizable normal-depth diffusion model for detail richness in text-to-3d. In *Proceedings of the IEEE/CVF conference on computer vision and pattern recognition*, pages 9914–9925, 2024.
- [55] Amit Raj, Srinivas Kaza, Ben Poole, Michael Niemeyer, Nataniel Ruiz, Ben Mildenhall, Shiran Zada, Kfir Aberman, Michael Rubinstein, Jonathan Barron, et al. Dreambooth3d: Subject-driven text-to-3d generation. In *Proceedings of the IEEE/CVF international conference on computer vision*, pages 2349–2359, 2023.
- [56] Nils Reimers and Iryna Gurevych. Sentencebert: Sentence embeddings using siamese bert-networks. *arXiv preprint arXiv:1908.10084*, 2019.
- [57] Gernot Riegler, Ali Osman Ulusoy, and Andreas Geiger. Octnet: Learning deep 3d representations at high resolutions. In *Proceedings of the IEEE conference on computer vision and pattern recognition*, pages 3577–3586, 2017.
- [58] Maarten Sap, Hannah Rashkin, Derek Chen, Ronan LeBras, and Yejin Choi. Socialliqa: Commonsense reasoning about social interactions. *arXiv preprint arXiv:1904.09728*, 2019.
- [59] Ruwen Schnabel and Reinhard Klein. Octree-based point-cloud compression. *PBG@ SIG-GRAPH*, 2006.
- [60] Zhihong Shao, Peiyi Wang, Qihao Zhu, Runxin Xu, Junxiao Song, Xiao Bi, Haowei Zhang, Mingchuan Zhang, YK Li, Yang Wu, et al. Deepseekmath: Pushing the limits of mathematical reasoning in open language models. *arXiv preprint arXiv:2402.03300*, 2024.
- [61] Ruoxi Shi, Hansheng Chen, Zhuoyang Zhang, Minghua Liu, Chao Xu, Xinyue Wei, Linghao Chen, Chong Zeng, and Hao Su. Zero123++: a single image to consistent multi-view diffusion base model. *arXiv preprint arXiv:2310.15110*, 2023.
- [62] Yichun Shi, Peng Wang, Jianglong Ye, Mai Long, Kejie Li, and Xiao Yang. Mvdream: Multi-view diffusion for 3d generation. *arXiv preprint arXiv:2308.16512*, 2023.
- [63] Yawar Siddiqui, Antonio Alliegro, Alexey Artemov, Tatiana Tommasi, Daniele Sirigatti, Vladislav Rosov, Angela Dai, and Matthias Nießner. Meshgpt: Generating triangle meshes with decoder-only transformers. In *Proceedings of the IEEE/CVF conference on computer vision and pattern recognition*, pages 19615–19625, 2024.
- [64] Jingxiang Sun, Bo Zhang, Ruizhi Shao, Lizhen Wang, Wen Liu, Zhenda Xie, and Yebin Liu. Dreamcraft3d: Hierarchical 3d generation with bootstrapped diffusion prior. *arXiv preprint arXiv:2310.16818*, 2023.
- [65] Richard Szeliski. Rapid octree construction from image sequences. *CVGIP: Image understanding*, pages 23–32, 1993.
- [66] Jiaxiang Tang, Jiawei Ren, Hang Zhou, Ziwei Liu, and Gang Zeng. Dreamgaussian: Generative gaussian splatting for efficient 3d content creation. *arXiv preprint arXiv:2309.16653*, 2023.
- [67] Jiaxiang Tang, Zhaoshuo Li, Zekun Hao, Xian Liu, Gang Zeng, Ming-Yu Liu, and Qinsheng Zhang. Edgerunner: Auto-regressive auto-encoder for artistic mesh generation. *arXiv preprint arXiv:2409.18114*, 2024.
- [68] Chameleon Team. Chameleon: Mixed-modal early-fusion foundation models. *arXiv preprint arXiv:2405.09818*, 2024. doi: 10.48550/

- arXiv:2405.09818. URL <https://github.com/facebookresearch/chameleon>.
- [69] Hugo Touvron, Thibaut Lavril, Gautier Izacard, Xavier Martinet, Marie-Anne Lachaux, Timothée Lacroix, Baptiste Rozière, Naman Goyal, Eric Hambro, Faisal Azhar, et al. Llama: Open and efficient foundation language models. *arXiv preprint arXiv:2302.13971*, 2023.
- [70] Aaron Van Den Oord, Oriol Vinyals, et al. Neural discrete representation learning. *Advances in neural information processing systems*, 30, 2017.
- [71] Vikram Voleti, Chun-Han Yao, Mark Boss, Adam Letts, David Pankratz, Dmitry Tochilkin, Christian Laforte, Robin Rombach, and Varun Jampani. Sv3d: Novel multi-view synthesis and 3d generation from a single image using latent video diffusion. In *European Conference on Computer Vision*, pages 439–457. Springer, 2024.
- [72] Haochen Wang, Xiaodan Du, Jiahao Li, Raymond A. Yeh, and Greg Shakhnarovich. Score jacobian chaining: Lifting pretrained 2d diffusion models for 3d generation. *arXiv preprint arXiv:2212.00774*, 2022.
- [73] Peng Wang and Yichun Shi. Imagedream: Image-prompt multi-view diffusion for 3d generation. *arXiv preprint arXiv:2312.02201*, 2023.
- [74] Peng-Shuai Wang. Octformer: Octree-based transformers for 3d point clouds. *ACM Transactions on Graphics (TOG)*, 42(4):1–11, 2023.
- [75] Peng-Shuai Wang, Yang Liu, Yu-Xiao Guo, Chun-Yu Sun, and Xin Tong. O-cnn: Octree-based convolutional neural networks for 3d shape analysis. *ACM Transactions On Graphics (TOG)*, pages 1–11, 2017.
- [76] Tengfei Wang, Bo Zhang, Ting Zhang, Shuyang Gu, Jianmin Bao, Tadas Baltrusaitis, Jingjing Shen, Dong Chen, Fang Wen, Qifeng Chen, et al. Rodin: A generative model for sculpting 3d digital avatars using diffusion. In *Proceedings of the IEEE/CVF conference on computer vision and pattern recognition*, pages 4563–4573, 2023.
- [77] Xinlong Wang, Xiaosong Zhang, Zhengxiong Luo, Quan Sun, Yufeng Cui, Jinsheng Wang, Fan Zhang, Yueze Wang, Zhen Li, Qiying Yu, et al. Emu3: Next-token prediction is all you need. *arXiv preprint arXiv:2409.18869*, 2024.
- [78] Xinzhou Wang, Yikai Wang, Junliang Ye, Zhengyi Wang, Fuchun Sun, Pengkun Liu, Ling Wang, Kai Sun, Xintong Wang, and Bin He. Animatabledreamer: Text-guided non-rigid 3d model generation and reconstruction with canonical score distillation. *arXiv preprint arXiv:2312.03795*, 2023.
- [79] Zhengyi Wang, Cheng Lu, Yikai Wang, Fan Bao, Chongxuan Li, Hang Su, and Jun Zhu. Prolificdreamer: High-fidelity and diverse text-to-3d generation with variational score distillation. *Advances in neural information processing systems*, 36:8406–8441, 2023.
- [80] Zhengyi Wang, Jonathan Lorraine, Yikai Wang, Hang Su, Jun Zhu, Sanja Fidler, and Xiaohui Zeng. Llama-mesh: Unifying 3d mesh generation with language models. *arXiv preprint arXiv:2411.09595*, 2024.
- [81] Jason Wei, Xuezhi Wang, Dale Schuurmans, Maarten Bosma, Fei Xia, Ed Chi, Quoc V Le, Denny Zhou, et al. Chain-of-thought prompting elicits reasoning in large language models. *Advances in neural information processing systems*, 35:24824–24837, 2022.
- [82] Si-Tong Wei, Rui-Huan Wang, Chuan-Zhi Zhou, Baoquan Chen, and Peng-Shuai Wang. Octgpt: Octree-based multiscale autoregressive models for 3d shape generation. In *Proceedings of the Special Interest Group on Computer Graphics and Interactive Techniques Conference Conference Papers*, pages 1–11, 2025.
- [83] Haohan Weng, Tianyu Yang, Jianan Wang, Yu Li, Tong Zhang, CL Chen, and Lei Zhang. Consistent123: Improve consistency for one

- image to 3d object synthesis. *arXiv preprint arXiv:2310.08092*, 2023.
- [84] Haohan Weng, Yikai Wang, Tong Zhang, CL Chen, and Jun Zhu. Pivotmesh: Generic 3d mesh generation via pivot vertices guidance. *arXiv preprint arXiv:2405.16890*, 2024.
- [85] Haohan Weng, Zibo Zhao, Biwen Lei, Xi-anhui Yang, Jian Liu, Zeqiang Lai, Zhuo Chen, Yuhong Liu, Jie Jiang, Chunchao Guo, et al. Scaling mesh generation via compressive tokenization. *arXiv preprint arXiv:2411.07025*, 2024.
- [86] Kailu Wu, Fangfu Liu, Zhihan Cai, Runjie Yan, Hanyang Wang, Yating Hu, Yueqi Duan, and Kaisheng Ma. Unique3d: High-quality and efficient 3d mesh generation from a single image. In *The Thirty-eighth Annual Conference on Neural Information Processing Systems*, 2024.
- [87] Shuang Wu, Youtian Lin, Feihu Zhang, Yifei Zeng, Jingxi Xu, Philip Torr, Xun Cao, and Yao Yao. Direct3d: Scalable image-to-3d generation via 3d latent diffusion transformer. *arXiv preprint arXiv:2405.14832*, 2024.
- [88] Xiaoshi Wu, Yiming Hao, Keqiang Sun, Yixiong Chen, Feng Zhu, Rui Zhao, and Hongsheng Li. Human preference score v2: A solid benchmark for evaluating human preferences of text-to-image synthesis. *arXiv preprint arXiv:2306.09341*, 2023.
- [89] Xiaoyang Wu, Li Jiang, Peng-Shuai Wang, Zhijian Liu, Xihui Liu, Yu Qiao, Wanli Ouyang, Tong He, and Hengshuang Zhao. Point transformer v3: Simpler faster stronger. In *Proceedings of the IEEE/CVF conference on computer vision and pattern recognition*, pages 4840–4851, 2024.
- [90] Jianfeng Xiang, Zelong Lv, Sicheng Xu, Yu Deng, Ruicheng Wang, Bowen Zhang, Dong Chen, Xin Tong, and Jiaolong Yang. Structured 3d latents for scalable and versatile 3d generation. *arXiv preprint arXiv:2412.01506*, 2024.
- [91] Jinheng Xie, Weijia Mao, Zechen Bai, David Junhao Zhang, Weihao Wang, Kevin Qinghong Lin, Yuchao Gu, Zhijie Chen, Zhenheng Yang, and Mike Zheng Shou. Show-o: One single transformer to unify multimodal understanding and generation. *arXiv preprint arXiv:2408.12528*, 2024.
- [92] Bojun Xiong, Jialun Liu, Jiakui Hu, Chenming Wu, Jinbo Wu, Xing Liu, Chen Zhao, Errui Ding, and Zhouhui Lian. Texgaussian: Generating high-quality pbr material via octree-based 3d gaussian splatting. In *Proceedings of the Computer Vision and Pattern Recognition Conference*, pages 551–561, 2025.
- [93] Jiazheng Xu, Xiao Liu, Yuchen Wu, Yuxuan Tong, Qinkai Li, Ming Ding, Jie Tang, and Yuxiao Dong. Imagereward: Learning and evaluating human preferences for text-to-image generation. *Advances in Neural Information Processing Systems*, 36:15903–15935, 2023.
- [94] Runsen Xu, Xiaolong Wang, Tai Wang, Yilun Chen, Jiangmiao Pang, and Dahua Lin. Pointllm: Empowering large language models to understand point clouds. In *European Conference on Computer Vision*, pages 131–147. Springer, 2024.
- [95] Le Xue, Mingfei Gao, Chen Xing, Roberto Martín-Martín, Jiajun Wu, Caiming Xiong, Ran Xu, Juan Carlos Niebles, and Silvio Savarese. Ulip: Learning a unified representation of language, images, and point clouds for 3d understanding. In *Proceedings of the IEEE/CVF conference on computer vision and pattern recognition*, pages 1179–1189, 2023.
- [96] Le Xue, Ning Yu, Shu Zhang, Artemis Panagopoulou, Junnan Li, Roberto Martín-Martín, Jiajun Wu, Caiming Xiong, Ran Xu, Juan Carlos Niebles, et al. Ulip-2: Towards scalable multimodal pre-training for 3d understanding. In *Proceedings of the IEEE/CVF Conference on Computer Vision and Pattern Recognition*, pages 27091–27101, 2024.
- [97] Yutaro Yamada, Khyathi Chandu, Yuchen Lin, Jack Hessel, Ilker Yildirim, and Yejin

- Choi. L3go: Language agents with chain-of-3d-thoughts for generating unconventional objects, 2024. URL <https://arxiv.org/abs/2402.09052>.
- [98] An Yang, Baosong Yang, Beichen Zhang, Binyuan Hui, Bo Zheng, Bowen Yu, Chengyuan Li, Dayiheng Liu, Fei Huang, Haoran Wei, et al. Qwen2. 5 technical report. *arXiv preprint arXiv:2412.15115*, 2024.
- [99] Xianghui Yang, Huiwen Shi, Bowen Zhang, Fan Yang, Jiacheng Wang, Hongxu Zhao, Xinhai Liu, Xinzhou Wang, Qingxiang Lin, Jiaao Yu, et al. Hunyuan3d 1.0: A unified framework for text-to-3d and image-to-3d generation. *arXiv preprint arXiv:2411.02293*, 2024.
- [100] Yi Yang, Xiaoxuan He, Hongkun Pan, Xiyan Jiang, Yan Deng, Xingtao Yang, Haoyu Lu, Dacheng Yin, Fengyun Rao, Minfeng Zhu, et al. R1-onevision: Advancing generalized multimodal reasoning through cross-modal formalization. *arXiv preprint arXiv:2503.10615*, 2025.
- [101] Chongjie Ye, Lingteng Qiu, Xiaodong Gu, Qi Zuo, Yushuang Wu, Zilong Dong, Liefeng Bo, Yuliang Xiu, and Xiaoguang Han. Stablenormal: Reducing diffusion variance for stable and sharp normal. *ACM Transactions on Graphics (TOG)*, 2024.
- [102] Chongjie Ye, Yushuang Wu, Ziteng Lu, Jiahao Chang, Xiaoyang Guo, Jiaqing Zhou, Hao Zhao, and Xiaoguang Han. Hi3dgen: High-fidelity 3d geometry generation from images via normal bridging. *arXiv preprint arXiv:2503.22236*, 3, 2025.
- [103] Junliang Ye, Fangfu Liu, Qixiu Li, Zhengyi Wang, Yikai Wang, Xinzhou Wang, Yueqi Duan, and Jun Zhu. Dreamreward: Text-to-3d generation with human preference. In *European Conference on Computer Vision*, pages 259–276. Springer, 2024.
- [104] Junliang Ye, Zhengyi Wang, Ruowen Zhao, Shenghao Xie, and Jun Zhu. Shapellm-omni: A native multimodal llm for 3d generation and understanding. *arXiv preprint arXiv:2506.01853*, 2025.
- [105] Taoran Yi, Jiemin Fang, Junjie Wang, Guan-jun Wu, Lingxi Xie, Xiaopeng Zhang, Wenyu Liu, Qi Tian, and Xinggang Wang. Gaussian-dreamer: Fast generation from text to 3d gaussians by bridging 2d and 3d diffusion models. In *Proceedings of the IEEE/CVF Conference on Computer Vision and Pattern Recognition*, pages 6796–6807, 2024.
- [106] Fukun Yin, Xin Chen, Chi Zhang, Biao Jiang, Zibo Zhao, Wen Liu, Gang Yu, and Tao Chen. Shapegpt: 3d shape generation with a unified multi-modal language model. *IEEE Transactions on Multimedia*, 2025.
- [107] Alex Yu, Ruilong Li, Matthew Tancik, Hao Li, Ren Ng, and Angjoo Kanazawa. Plenotrees for real-time rendering of neural radiance fields. In *Proceedings of the IEEE/CVF international conference on computer vision*, pages 5752–5761, 2021.
- [108] Tianjiao Yu, Vedant Shah, Muntasir Wahed, Ying Shen, Kiet A Nguyen, and Ismini Lourentzou. Part²GS: Part-aware modeling of articulated objects using 3d gaussian splatting. *arXiv preprint arXiv:2506.17212*, 2025.
- [109] Jingyi Zhang, Jiaying Huang, Huanjin Yao, Shunyu Liu, Xikun Zhang, Shijian Lu, and Dacheng Tao. R1-vl: Learning to reason with multimodal large language models via step-wise group relative policy optimization. *arXiv preprint arXiv:2503.12937*, 2025.
- [110] Longwen Zhang, Ziyu Wang, Qixuan Zhang, Qiwei Qiu, Anqi Pang, Haoran Jiang, Wei Yang, Lan Xu, and Jingyi Yu. Clay: A controllable large-scale generative model for creating high-quality 3d assets. *ACM Transactions on Graphics (TOG)*, 43(4):1–20, 2024.
- [111] Renrui Zhang, Dongzhi Jiang, Yichi Zhang, Haokun Lin, Ziyu Guo, Pengshuo Qiu, Aojun Zhou, Pan Lu, Kai-Wei Chang, Yu Qiao, et al.

Mathverse: Does your multi-modal llm truly see the diagrams in visual math problems? In *European Conference on Computer Vision*, pages 169–186. Springer, 2024.

- [112] Renrui Zhang, Xinyu Wei, Dongzhi Jiang, Yichi Zhang, Ziyu Guo, Chengzhuo Tong, Jiaming Liu, Aojun Zhou, Bin Wei, Shanghang Zhang, et al. Mavis: Mathematical visual instruction tuning. *arXiv preprint arXiv:2407.08739*, 2024.
- [113] Ruowen Zhao, Zhengyi Wang, Yikai Wang, Zihan Zhou, and Jun Zhu. Flexidreamer: single image-to-3d generation with flexicubes. *arXiv preprint arXiv:2404.00987*, 2024.
- [114] Ruowen Zhao, Junliang Ye, Zhengyi Wang, Guangce Liu, Yiwen Chen, Yikai Wang, and Jun Zhu. Deepmesh: Auto-regressive artist-mesh creation with reinforcement learning. *arXiv preprint arXiv:2503.15265*, 2025.
- [115] Zibo Zhao, Wen Liu, Xin Chen, Xianfang Zeng, Rui Wang, Pei Cheng, Bin Fu, Tao Chen, Gang Yu, and Shenghua Gao. Michelangelo: Conditional 3d shape generation based on shape-image-text aligned latent representation. *Advances in neural information processing systems*, 36:73969–73982, 2023.
- [116] Chunting Zhou, Lili Yu, Arun Babu, Kushal Tirumala, Michihiro Yasunaga, Leonid Shamis, Jacob Kahn, Xuezhe Ma, Luke Zettlemoyer, and Omer Levy. Transfusion: Predict the next token and diffuse images with one multi-modal model. *arXiv preprint arXiv:2408.11039*, 2024.
- [117] Ziyu Zhu, Xiaojian Ma, Yixin Chen, Zhidong Deng, Siyuan Huang, and Qing Li. 3d-vista: Pre-trained transformer for 3d vision and text alignment. In *Proceedings of the IEEE/CVF International Conference on Computer Vision*, pages 2911–2921, 2023.

A. Additional Related Work

Post-Pretraining Reinforcement Learning. Since the introduction of Chain-of-Thought prompting [81], enhancing the reasoning ability of large language models has become an important research focus. More recently, DeepSeek-R1 [26] advanced this direction by proposing a rule-based reward design combined with GRPO training, encouraging models to produce explicit intermediate reasoning traces before generating final answers. This paradigm has since been extended to multimodal settings [31, 50, 100, 109], where task-specific rewards guide the learning process. These reasoning-driven methods have achieved notable gains across a variety of challenging tasks [46], including mathematical problem solving [111, 112] and code generation [33, 42]. Our proposed **CoRe3D** framework builds on this line of work by extending GRPO from text-only settings to a unified 3D understanding and 3D generation model. We employ a collaborative reasoning strategy that tightly couples linguistic semantics with 3D geometry, leading to more coherent and interpretable generation.

Octant-based 3D Representations. The concept of octree has been used in a wide range of 3D geometric processing applications, including point cloud compression [59], 3D texturing [5, 92], and multi-view scene reconstruction [65, 107]. Beyond these foundational uses, octree structures have become integral to efficient shape analysis in large-scale environments [25, 57, 74, 75, 89]. In the realm of generative modeling, recent advancements [22, 22, 82] employ adaptive tokenization or multi-scale autoregressive strategies to allocate computational resources to geometrically complex regions dynamically. Diverging from these adaptive hierarchical methods, which often result in variable-length sequences or complex tree traversals, our approach utilizes a fixed-resolution octant-based 3D VQ-VAE to discretize the 3D volume into uniform blocks. This design preserves essential spatial locality while maintaining a compact token sequence, thereby facilitating stable and interpretable geometric chain-of-thought reasoning within a unified 3D-LLM framework.

B. Implementation Details

Octant-based Auto-regressive Model. Autoregressive generation over 3D volumetric representations poses a unique challenge: the model must preserve spatial locality while maintaining a tractable token length. Traditional raster-order serialization severely disrupts locality in 3D, making next-token prediction unnecessarily difficult. Inspired by ideas from hierarchical octant-based models such as OctFormer [74] and OctGPT [82], we adopt an octant-structured tokenization strategy tailored to our VQ-VAE latent space. Unlike hierarchical octrees, our formulation operates on a single-scale 16^3 latent grid while preserving the locality benefits emphasized in prior octant-based architectures.

As shown in Figure 8, our voxel VQ-VAE maps each 64^3 input volume to a 16^3 latent grid. To reduce sequence length while preserving local geometric structure, we partition this latent grid into non-overlapping $2 \times 2 \times 2$ neighborhoods. Each neighborhood forms a local *octant block* that contains eight spatially adjacent latent cells. Concatenating the features of these eight cells produces a single octant token, yielding exactly $8 \times 8 \times 8 = 512$ tokens per object. These tokens summarize compact spatial regions and maintain local geometry and appearance cues.

To serialize the latent volume into an autoregressive sequence, we employ a Morton (Z-order) space-filling curve, which preserves spatial locality more effectively than raster or lexicographic scanning. Let $\mathcal{O} = [o_1, o_2, \dots, o_{512}]$ denote the sequence of octant tokens arranged in Morton order. The generative process factorizes the distribution over the latent volume as

$$p(\mathcal{O}) = \prod_{i=1}^{512} p(o_i \mid o_{<i}, \mathcal{S}_{\text{sem}}), \quad (6)$$

where the semantic chain-of-thought \mathcal{S}_{sem} provides high-level cues that guide geometric synthesis.

To encode spatial location, we attach a learned positional embedding to each octant token, keyed by its block index (x_b, y_b, z_b) in the $8 \times 8 \times 8$ grid. This embedding is injected *after* vector quantization, ensuring that the codebook remains content-centric while the autoregressive decoder remains location-

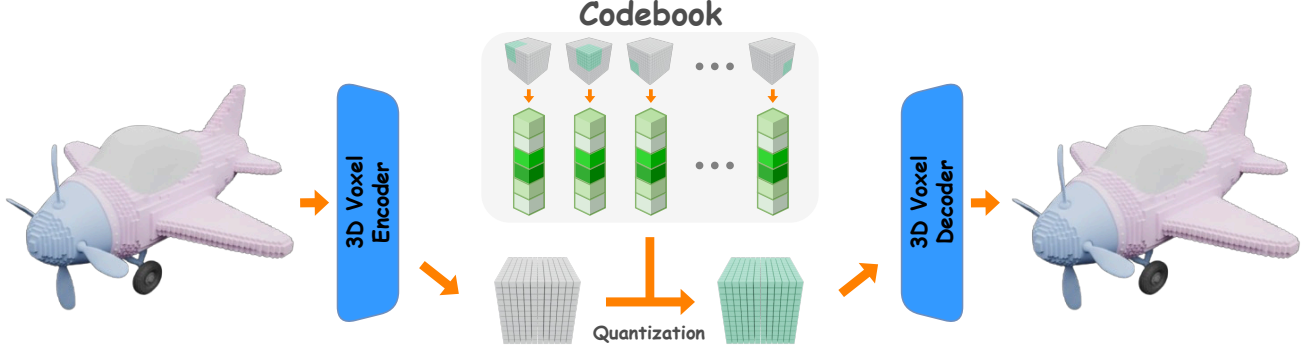


Figure 8: Overview of Octant-based 3D VQVAE. The voxelized geometry is encoded into latent blocks, quantized using a shared codebook of 3D embeddings, and decoded back into a high-fidelity voxel grid.

aware. Together, the octant blocks and positional embeddings introduce two inductive biases: (i) each token carries high-resolution local geometric context, and (ii) the sequence ordering respects 3D locality.

During training, the semantic reasoning trace \mathcal{S}_{sem} and the geometric reasoning trace \mathcal{G}_{geo} jointly condition the autoregressive transformer. The semantic trace encodes global planning information such as categories and textures, while the geometric trace provides localized structural cues for neighborhood-level voxel refinement. The decoder predicts a discrete codebook index for each octant token, reconstructing the latent volume block-by-block. After predicting all 512 tokens, the VQ-VAE decoder reconstructs a dense 64^3 voxel field, which is subsequently rendered into mesh or multi-view images. Compared to hierarchical octree models [82], which must autoregressively generate thousands of binary split or leaf tokens, our design yields a significantly shorter and more expressive sequence. This compact, locality-aware autoregressive formulation is essential to our framework, enabling efficient token-level generation that tightly aligns with semantic and geometric reasoning.

Physical Coherence Critic. We use TRIMESH to compute physical statistics and PyMESHFix to diagnose self-intersections. Stability is estimated by projecting the mesh center of mass onto the ground plane and checking whether this projection lies inside the convex hull of bottom support vertices extracted from the lowest- z region, yielding a normalized stability score. Structural connectivity is measured by split-

ting the mesh into connected components and computing the fraction of faces belonging to the largest component, which penalizes fragmented or floating parts. To assess self-intersection, we run PyMESHFix on the original mesh and compare the number of faces before and after repair; a larger relative change indicates more severe geometric artifacts and results in a lower self-intersection score.

Hyperparameters. The policy is updated using KL-regularized GRPO with ratio clipping. The KL penalty coefficient is set to $\beta = 0.01$ and the clipping threshold to $\varepsilon = 0.1$. For each prompt, we sample $K=4$ candidate generations and compute pairwise preferences using the four critics introduced in §3. The human-preference, 3D-understanding, Text-3D-alignment, and Physical coherence critics are weighted by $(w_H, w_V, w_X, w_P) = (0.25, 0.25, 0.25, 0.25)$. Optimization uses AdamW with a learning rate of 1×10^{-6} , $\beta_1=0.9$, $\beta_2=0.98$, and weight decay 0.01. We apply a 2000-step linear warmup followed by cosine decay. For stability, the policy KL is capped at $1.2\times$ its exponential moving average, and gradients are clipped with a global norm of 1.0.

Evaluation Metrics. We report common text-generation metrics, *i.e.*, BLEU-1 [51], ROUGE-L [38], and METEOR [4]. Although standard, these metrics often favor shorter outputs and may overlook semantic fidelity. To address this, we incorporate embedding-based similarity measures, including Sentence-BERT [56] and SimCSE [23], which evaluate semantic alignment between generated captions and human references more robustly.





Input Text	Semantic-CoT	CoRe3D
<i>A wooden female figure that can be opened multiple times</i>	<i>A smooth, rounded wooden shell that ... The internal hierarchy of decreasing sizes should follow the traditional structure of a Matryoshka doll ...</i>	
<i>A round baked pastry with a golden-brown representing the moon</i>	<i>Start by shaping a compact, circular pastry with ... spherical center to reflect the symbolic salted-yolk core seen in traditional mooncakes. The cross-section should maintain a clean...</i>	
<i>A tall metal tower often associated with French</i>	<i>Model a tall, tapering metal structure ... reproducing the familiar proportions of the Eiffel Tower in miniature form. The geometry should emphasize beam patterns and structural symmetry...</i>	
<i>A folded figure made from crisp paper often representing peace</i>	<i>Begin with crisp, angular planes representing folded paper... The overall form should preserve the faceted, single-sheet structure characteristic of a paper crane.</i>	

Figure 9: Additional Results on Challenging Prompts. CoRe3D successfully inferred the true object from the implicit prompts.

C. Additional Results

Additional Results on Challenging Prompts. Figure 9 presents additional qualitative examples demonstrating CoRe3D’s ability to infer the correct 3D object even when the input prompt provides only indirect or symbolic descriptions. These prompts intentionally avoid naming the target object and instead describe cultural context, functional cues, or high-level visual impressions. Despite this ambiguity, CoRe3D consistently recovers the correct underlying structure. As shown, the model not only identifies the implicit object but also reconstructs a spatially coherent and visually faithful 3D shape.

To our knowledge, CoRe3D is the first 3D generative framework capable of resolving such implicit, referential prompts through semantic reasoning, rather than relying on explicit object mentions or category supervision.

Quantitative Results of Semantic-CoT and Geometric CoT Ablation. We conduct a quantitative analysis to isolate the contributions of the two

complementary reasoning CoTs. As shown in Table 5, introducing **Semantic CoT** yields the largest gains in 3D captioning quality, improving METEOR, Sentence-BERT, and SimCSE scores by a significant margin over ShapeLLM-Omni. This indicates that explicit semantic reasoning helps the model better decompose text prompts into linguistically grounded object attributes. In contrast, **Geometric CoT** primarily benefits 3D generation. By encouraging structured spatial reasoning over octant-level geometry, it substantially improves CLIP similarity and reduces both FD and KD, demonstrating its effectiveness in guiding the model toward globally coherent 3D shapes. Our full model, **CoRe3D**, achieves the best overall performance across all metrics. These results verify that collaborative reasoning is essential for robust 3D understanding and generation.

Comparison with Zero-shot CoT. Figure 10 and Figure 11 compare our trained semantic-level CoT with a zero-shot CoT baseline (Qwen2.5-vl-7B[3]). In the zero-shot setting, the model is prompted to produce a free-form structural description before generating the 3D object, but this unguided semantic reasoning pro-

Table 5: Ablation of Semantic CoT and Geometric CoT. Best and second-best results are highlighted.

Model Name	Critic		3D Captioning			3D Generation		
	Semantic CoT	Geometric CoT	METEOR ↑	Sentence-BERT ↑	SimCSE ↑	CLIP ↑	FD _{incep} ↓	KD _{incep} ↓
ShapeLLM-Omni	✗	✗	12.76	44.91	48.14	0.29	23.4	0.25
CoRe3D (w/o Geometric CoT)	✓	✗	16.42	50.38	51.14	0.32	21.6	0.21
CoRe3D (w/o Semantic CoT)	✗	✓	14.89	47.32	50.41	0.35	19.8	0.19
CoRe3D (Ours)	✓	✓	17.03	49.67	52.11	0.38	18.7	0.17

Table 6: Ablation of Octant Depth in the Octant-based 3D VQ-VAE. Increasing depth increases spatial granularity (8 → 4096 octants) and improves fidelity up to Depth 3, after which autoregressive instability degrades performance. Best and second-best.

Architecture		3D Captioning			3D Generation		
Depth	# Octants	METEOR ↑	SBERT ↑	SimCSE ↑	CLIP ↑	FD _{incep} ↓	KD _{incep} ↓
1	8	7.34	41.82	43.10	0.21	42.3	0.34
2	64	12.87	46.51	47.88	0.29	29.4	0.25
3 (Ours)	512	17.03	49.67	52.11	0.38	18.7	0.17
4	4096	16.44	49.92	51.36	0.37	19.0	0.18

vides only shallow, low-information descriptions. For instance, in the “compact car” example, the zero-shot CoT yields a generic outline of a smooth white prototype with no color, style cues, or structural modifiers, leading to an oversimplified reconstruction. In contrast, the CoRe3D semantic-level CoT produces richer and more actionable structural cues, such as bright blue body color, semi-transparent windows, stylized panel lines, or the presence of a roof rack with parallel bars and a fin-like rear element (bottom CoT row), and the model correspondingly reconstructs a much more faithful 3D shape. These results show that zero-shot CoT lacks the necessary semantic grounding for 3D generation, whereas CoRe3D learns to produce CoT that is both structurally informative and tightly aligned with the generation process. This highlights the necessity of our collaborative reasoning pipeline.

Additional Image-to-3D Results. Figure 12 shows additional qualitative results from our image-to-3D pipeline. Despite being a unified model rather than a specialized reconstruction system, CoRe3D generates stable and coherent 3D shapes even from visually complex or cluttered inputs. The model maintains globally consistent geometry, plausible spatial structure, and strong color fidelity, delivering reconstructions that capture the essential form, material cues, and overall visual identity of the input objects.

Optimal Octant Layers. Table 6 evaluates how the

Table 7: Ablation of Codebook Size in the Octant-based 3D VQ-VAE. Larger codebooks reduce quantization error but exhibit diminishing returns and instability at extreme scales. Octant depth is fixed at 512 octants (Depth 3). Best and second-best.

Architecture		3D Captioning			3D Generation		
Codebook Size	Octants	METEOR ↑	SBERT ↑	SimCSE ↑	CLIP ↑	FD _{incep} ↓	KD _{incep} ↓
2048	512	13.81	46.92	47.44	0.31	27.8	0.24
4096	512	15.92	48.51	50.03	0.34	22.1	0.20
8192 (Ours)	512	17.03	49.67	52.11	0.38	18.7	0.17
16384	512	16.77	49.98	51.62	0.37	19.3	0.18

choice of octant depth and therefore the total number of octant tokens affects the performance of our octant-based 3D VQ-VAE. Increasing the depth refines the spatial partitioning of the latent volume (from 8 to 4096 octants), granting the model access to progressively finer geometric detail. We observe a consistent upward trend from Depth 1 to Depth 3 across all captioning and generation metrics. Depth 1 (only 8 octants) severely under-parameterizes local geometry, leading to weak semantic alignment and the worst FD/KD scores. Depth 2 (64 octants) recovers coarse global structure but still lacks local detail, resulting in moderate improvements. Depth 3 provides the best balance between spatial granularity and autoregressive stability. It achieves the highest scores for METEOR, SimCSE, CLIP, and the lowest FD/KD, demonstrating that this level of decomposition offers enough local resolution to capture high-frequency geometry without excessively lengthening the autoregressive sequence. We use Depth 3 as our default. At Depth 4, although the finer subdivision (4096 octants) slightly improves SBERT similarity and CLIP alignment, overall performance begins to degrade.

Optimal Codebook Size. Table 7 evaluates how the capacity of the VQ-VAE codebook affects both semantic alignment and 3D generation fidelity. A small codebook (2048 entries) creates a severe quantization bottleneck. This under-expressiveness leads to noticeably lower METEOR, SBERT, and

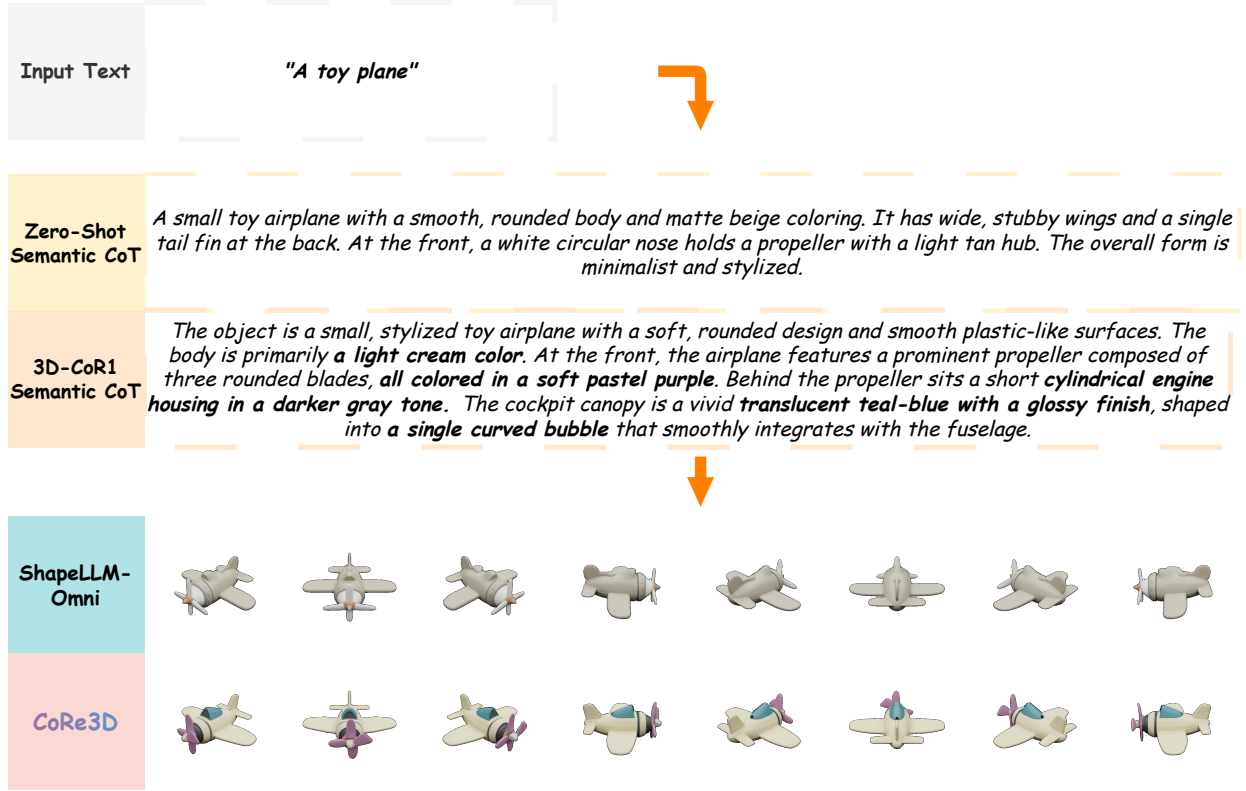


Figure 10: Comparison with Zero-shot CoT. Zero-shot CoT produces shallow, generic structural descriptions, leading to oversimplified 3D shapes.

SimCSE scores, along with substantially worse FD/KD metrics. Increasing the codebook to 4096 entries alleviates this issue and yields consistent gains across all evaluation dimensions. Our default setting with an 8192-entry codebook achieves the best overall performance. Expanding the codebook further to 16384 entries results in only marginal improvements on SBERT and CLIP similarity, but degrades generation fidelity. These findings indicate that our 8192-entry codebook is the optimal.

D. Broader Impacts

CoRe3D advances unified 3D intelligence by enabling models to both *interpret* and *construct* 3D objects through collaborative semantic-geometric-reasoning. Such capabilities can benefit a wide spectrum of applications. In robotics and embodied AI, improved spatial reasoning may support better manipulation, affordance understanding, and task planning. In simulation and digital twin systems, controllable 3D gen-

eration can streamline asset creation and accelerate workflows in engineering and education.

At the same time, such frameworks carry several potential risks. Unified 3D models may unintentionally reproduce private or proprietary content, and generative pipelines could be misused to create realistic yet deceptive 3D assets. CoRe3D is intended for research and educational use, and we encourage responsible deployment that emphasizes transparency, provenance tracking, consent for training data, and adherence to domain-specific usage guidelines. With such measures in place, we believe the benefits of collaborative reasoning for 3D understanding and generation outweigh the potential risks.

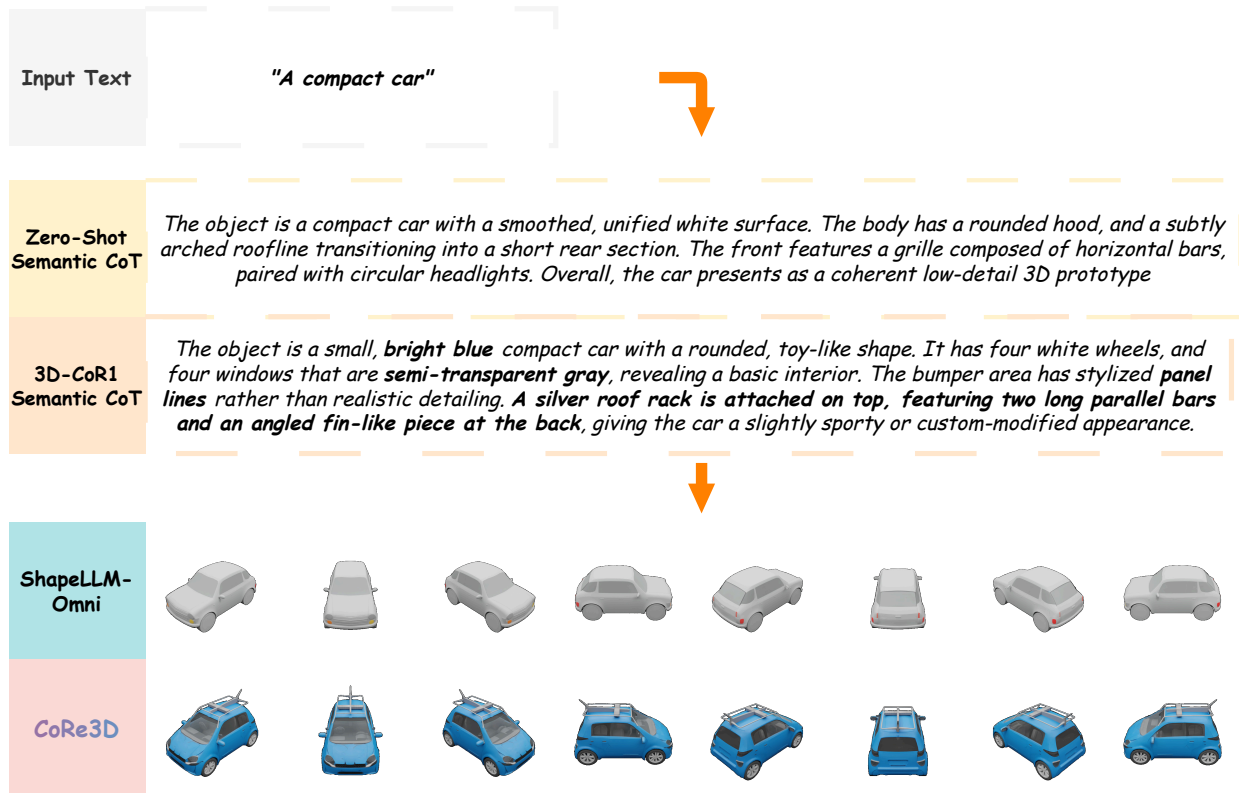


Figure 11: Comparison with Zero-shot CoT (2). Another example showing that zero-shot CoT provides limited guidance, while our trained semantic-level CoT yields detailed structural cues.

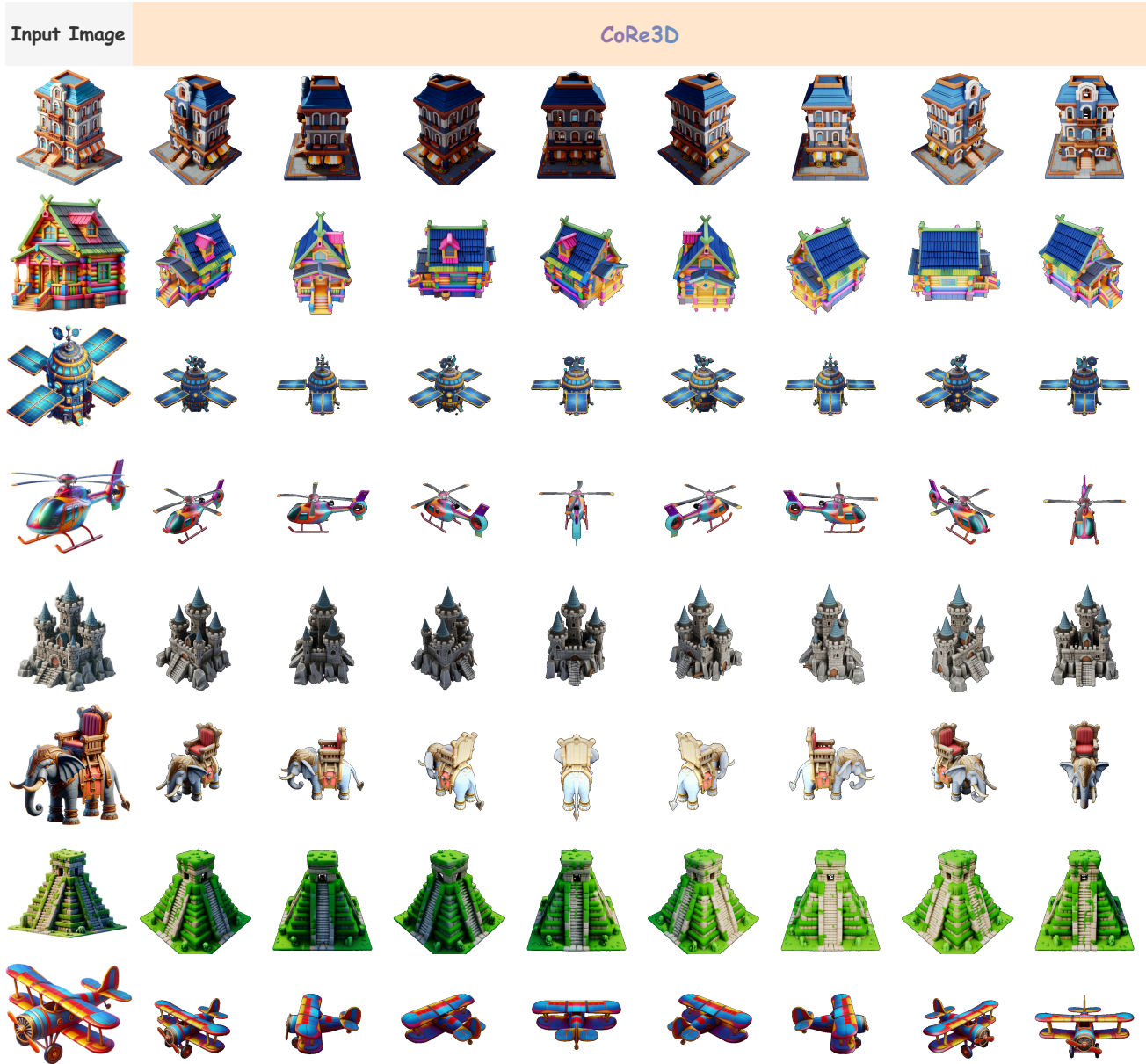


Figure 12: Additional Image-to-3D Results. We use visually complex image prompts to demonstrate that CoRe3D achieves strong 3D reconstruction capability, producing coherent geometry and spatially consistent shapes even for challenging inputs.